Journal of Orthopaedic Translation 52 (2025) 97–115

Contents lists available at ScienceDirect

Journal of Orthopaedic Translation

journal homepage: www.journals.elsevier.com/journal-of-orthopaedic-translation

Original Article

PDGF-BB improves cortical bone quality through restoring the osteogenic microenvironment in the steroid-associated osteonecrosis of rabbits

Huijuan Cao [a,b,d,*,1], Keda Shi [a,1], Jing Long [a,d], Yanzhi Liu [a,e], Xiangbo Meng [a,d], Cuishan Huang [a,d], Jie Hao [a], Lingli Li [a], Yiqing Zhao [a], Tianluo Ye [a], Yuxiao Lai [a,d], Ling Qin [a,c,d,**], Xinluan Wang [a,b,d,***]

[a] Centre for Translational Medicine Research & Development, Shenzhen Institutes of Advanced Technology, Chinese Academy of Sciences, Shenzhen, PR China
[b] Key Laboratory of Biomedical Imaging Science and System, Chinese Academy of Sciences, PR China
[c] Musculoskeletal Research Laboratory, Department of Orthopaedics & Traumatology, The Chinese University of Hong Kong, Hong Kong Special Administrative Region of China
[d] Joint Laboratory of Chinese Academic of Science and Hong Kong for Biomaterials of the Chinese University of Hong Kong Shenzhen, Shenzhen, PR China
[e] Guangdong Key Laboratory for Research and Development of Natural Drugs, Department of Pharmacology, Guangdong Medical University, Zhanjiang, PR China

ARTICLE INFO

Keywords:
PDGF-BB
SAON
Femoral diaphysis
Bone remodeling

ABSTRACT

Objective: Steroid-associated osteonecrosis of the femoral head (SONFH) is a refractory disease characterized by progressive bone destruction. Clinical evidence suggests that SONFH may extend beyond the intra-capital region to the femoral neck, metaphysis, and even diaphysis, increasing the risk of subtrochanteric fractures and implant loosening post-surgery. While our previous study demonstrated that platelet-derived growth factor-BB (PDGF-BB) promotes reparative osteogenesis in the femoral head, its effects on cortical bone quality in the extended diaphyseal regions under steroid-associated osteonecrosis (SAON) remain unclear. This study aims to investigate whether PDGF-BB could mitigate cortical bone deterioration in the femoral diaphysis during SAON progression.
Methods: SAON was induced by repeated lipopolysaccharide (LPS) and methylprednisolone (MPS) injections in rabbits. At 2, 4, and 6 weeks after SAON induction, PDGF-BB was intramedullary injected into the proximal femur. Xylenol orange and Calcein green were injected subcutaneously into rabbits on days 14 and 4 before euthanasia. At 3 days after last PDGF-BB treatment, micro-fil perfusion was performed for angiography. Then the femur shaft was dissected for micro-computed tomography (μCT)-based angiography, μCT-based cortical bone geometry, and histological analysis. With regard to the macrophage infiltration and activated osteoclast function in osteonecrosis regions during SAON progression, RAW 264.7 cells were utilized to evaluate the effect of PDGF-BB on macrophage polarization and osteoclasts activity *in vitro*.
Results: In this study, osteonecrosis extended to the femoral diaphysis, accompanied by vascular disruption (reduced CD31+ vessels), sensory nerve degeneration (decreased CGRP + fibers), and cortical bone destruction, at 6 weeks post-SAON induction. While PDGF-BB treatment significantly attenuated SAON progression in the femoral diaphysis, restoring blood supply (angiography) and improving cortical bone geometry (μCT). Histologically, PDGF-BB enhanced periosteal and endosteal osteogenesis while suppressing osteoclastic resorption. *In vitro,* PDGF-BB not only could modulate M1-type macrophages polarization to reduce inflammatory response, but also subsequently afford a secondary source of bioactivity factors during osteoclasts formation process to restore the osteogenic microenvironment, suggesting a dual role in resolving inflammation and enhancing bone remodeling.
Conclusion: SAON progression leads to diaphyseal cortical bone deterioration, while PDGF-BB application could restore the osteogenic microenvironment and drive cortical bone remodeling during SAON progression.

* Co-corresponding author. Shenzhen University Town, 1068 Xueyuan Avenue, Shenzhen, Guangdong, PR China.
** Corresponding author. Department of Orthopaedics & Traumatology, The Chinese University of Hong Kong, Prince of Wales Hospital, 5/F Lui Che Woo Clinical Sciences Building, Shatin, N.T., Hong Kong Special Administrative Region of China.
*** Corresponding author. Shenzhen University Town, 1068 Xueyuan Avenue, Shenzhen, Guangdong, PR China.
E-mail addresses: hj.cao@siat.ac.cn (H. Cao), lingqin@cuhk.edu.hk (L. Qin), xl.wang@siat.ac.cn (X. Wang).
[1] These authors contributed equally as first author to this work.

https://doi.org/10.1016/j.jot.2025.03.010
Received 9 October 2024; Received in revised form 16 February 2025; Accepted 21 March 2025
2214-031X/© 2025 The Authors. Published by Elsevier B.V. on behalf of Chinese Speaking Orthopaedic Society. This is an open access article under the CC BY-NC-ND license (http://creativecommons.org/licenses/by-nc-nd/4.0/).

The translational potential of this article: These findings suggest that PDGF-BB could serve as a potential candidate for attenuating the progression of SAON. Local delivery of PDGF-BB during surgical interventions for SONFH may enhance cortical bone repair and improve mechanical stability, offering a clinically viable strategy to achieve better long-term outcomes.

1. Introduction

High dose/excessive glucocorticoids (GCs) are widely used in many medical conditions, including severe infections like sepsis, acute respiratory distress syndrome, community-acquired pneumonia, and autoimmune diseases such as rheumatoid arthritis [1,2]. While high-dose GC therapy effectively modulates inflammation and mitigates cytokine storm-induced organ damage, it is also strongly associated with an increased risk of steroid-associated osteonecrosis (SAON), particularly affecting the major weight-bearing hip joint, a condition known as steroid-associated osteonecrosis of femoral head (SONFH) [3,4]. This condition can lead to progressive hip damage and a high rate of disability [5,6]. Hip preservation surgeries, such as core decompression (CD) combines with bone grafting, are commonly used to delay femoral head collapse in SONFH patients [7]. However, despite these interventions, a significant proportion of SONFH patients eventually require total hip arthroplasty (THA), with reports indicating that 5–18 % of annual THA procedures are performed for SONFH [8]. Notably, these patients may face additional risks, such as subtrochanteric fracture following CD [7,9], as well as periprosthetic fractures during THA or failure to femoral stem osseointegration [10,11]. These complications highlight the critical role of cortical bone quality in the femur shaft for the success of both CD and THA procedures. Histological evidence suggests that SONFH not only affects the intra-capital region but may also extend into the femoral neck, metaphyseal, and even the diaphysis [12]. When the osteonecrotic lesions extend into the diaphyseal region, cortical bone turnover and remodeling may be compromised, potentially impairing long-term implant fixation. So, implants placed within or near pathological bone are at risk of poor osteointegration and suboptimal outcomes [8,12]. However, the pathological characteristics in the femoral diaphysis under SAON condition remain poorly understood.

Platelet-derived growth factor BB (PDGF-BB) is a Food and Drug Administration (FDA) approved therapeutic agent for bone defects, known for its roles in angiogenesis, osteogenesis, and mesengenesis during bone repair [13,14]. PDGF-BB activates the PDGF receptors α and β (PDGFRα and PDGFRβ) signaling axis, supporting the sequential phases of bone healing, including inflammation, tissue formation, remodeling, and maturation [15]. Recent studies have confirmed that PDGF-BB extrinsically regulates the fate determination of both bone marrow mesenchymal stem cells (BMSCs) and periosteum-derived cells (PDCs), both of which contribute to osteogenesis in skeletal system [16,17]. However, high dose/excessive GCs use is known to downregulate PDGF-BB expression, consequently impairing the endogenous regenerative capacity of bone [18]. Data from GEO (GSE123568) reveal lower translation level of PDGF-BB in peripheral blood mononuclear cells of SONFH patients compared with non-SONFH patients (Fig. S1). Similarly, a decrease in PDGFRβ level has been observed in the mid-stage of SONFH patients [19]. Our previous studies have shown the low levels of bone marrow endothelial progenitor cells (EPCs) and MSCs contribute to destructive repair in SAON, which associated with rapid progression of hip damage [20]. Furthermore, in these destructive repair areas, the level of PDGF-BB was significantly lower compared to that in reparative osteogenesis areas of SAON [21]. Supplement recombinant PDGF-BB into the proximal femur promotes reparative osteogenesis in the femoral head by enhancing type H ($CD31^{hi}Emcn^{hi}$) vessel formation and leptin receptor-positive (LepR+) MSCs proliferation in SAON rabbits [21]. However, it remains uncertain whether PDGF-BB supplementation can also improve cortical bone quality in the femoral diaphysis under SAON conditions.

Rabbits are the most commonly used animal model for studying pathogenesis and pathophysiology of SAON, and it was reported that the fracture toughness of the rabbit femur shaft is comparable to that of human [22]. Especially, rabbits posses an active Haversian canal system in cortical bone [23,24], making them an ideal model for investigating cortical bone pathophysiology in the femur shaft [23]. In this study, we used a previously established protocol to induce SAON in rabbits through repeated lipopolysaccharide (LPS) and methylprednisolone (MPS) injections [21]. SAON rabbits were then treated with PDGF-BB to evaluate its potential to drive periosteal and endosteal osteogenesis in cortical bone under SAON condition. Chronic inflammation is a hallmark of SAON, and unresolved inflammation can lead to progressive bone destruction [5]. Our previous studies have demonstrated significant macrophage infiltration in the SAON-affected regions, with an increased ratio of M1 to M2 macrophages as SAON progression and accompanied by elevated levels of proinflammatory factors and enhanced osteoclastic bone resorption [25]. With regard to the pathological features of SAON as above, we used the macrophages line RAW 264.7 cells to further investigate the effect of PDGF-BB on regulating the inflammatory response and osteoclast activity *in vitro*.

2. Methods

2.1. Establishing the SAON rabbit model

Forty 16-weeks-old male New Zealand white rabbits weighing 2.0–2.2 kg were purchased from Guangdong Medical Laboratory Animal Center (Guangzhou, China) and maintained in a common facility at Shenzhen-Peking University-Hong Kong University of Science & Technology (Shenzhen-PKU-HKUST) Medical Center. All procedures were approved by the Institutional Animal Care and Use Committee of the Shenzhen Institute of Advanced Technology, Chinese Academy of Sciences (SIAT-IRB-150308-YGS-CHJ-A0140). After housing for 4 weeks, thirty rabbits (weighing 2.0–2.5 kg) were used to establish the SAON rabbit model [21]. In brief, an intravenous injection of 10 μg/kg lipopolysaccharide (LPS, *Escherichia coli* O111:B4, Sigma–Aldrich, St. Louis, MO, USA) was administered on days 0 and 14, followed by intramuscular injections of 20 mg/kg methylprednisolone (MPS, Pfizer, Peapack, NJ, USA) on days 1, 2, and 3, and on days 15, 16, and 17. The SAON rabbits were randomly divided into three groups. After first LPS injection, 1 μg/dose or 2 μg/dose rhPDGF-BB (100-14B, PeproTech, Rocky Hill, NJ, USA) was delivered in protein form by intramedullary injection into the proximal femora at 2, 4, and 6 weeks, respectively (Fig. 4A). Ten untreated rabbits were used as normal control. At 3 days after the last drug treatment, the femora of the rabbits were collected.

PDGF-BB is a dimer composed of two PDGF-B subunits [26]. A comparison of the full amino acid (AA) sequences of PDGF-B subunits between humans and rabbits reveals that AA sequences exhibit a high degree of homology, the primary three-dimensional (3D) structure of the AA in the PDGF-B subunit are conserved between the two species (Fig. S2). This structural conservation supports the use of the rabbit model in this study to evaluate the effects of rhPDGF-BB. In the present experimental study, the dosages of rhPDGF-BB were designed based on our published work [21].

2.2. Micro-CT-based cortical bone mineral density and bone architecture evaluation

After euthanasia, bilateral femora of the rabbits were collected and

then fixed in 10 % formalin (DF0111, League, Anhui, China) for 1 week. μCT (Skyscan 1176; Bruker, Belgium) with a spatial resolution of 18 μm was used to scan the middle cortical bone in the femur shaft at 66 kV and 110 μA. Mineralized tissue was separated from the background signal using an Al 1.0 filter which was defined by a threshold of more than 80 HU. The middle cortical bone (2 mm) of the femur shaft was selected as the region of interest (ROI), and then the 3D structure of the ROI was reconstructed and analyzed using a CT-Analyzer. Quantitative 2D and 3D analysis results showed Tissue areas (T.Ar, mm^2) and Bone areas (B. Ar, mm^2), Periosteum perimeter (Ps.Pm, mm), Endosteum perimeter (Es.Pm, mm), Radius of cortical bone (Rm, mm), volumetric bone mineral density (vBMD, g/cm^3), and the mean polar moment of inertia (pMOI, mm^4). The strength strain index (SSI, mm^3) was calculated for cortical bone as a published calculation method [27]. SSI=Normalized BMD × 1/Rm × pMOI. Normalized BMD: vBMD/Normal vBMD.

2.3. Micro-CT-based angiography for vascular architecture evaluation

General and deep anesthesia was induced in rabbits by intravenously administering 3–5 ml of 3 % sodium pentobarbital (P11011, Merk, San Diego, CA, USA). The abdominal cavities of the rabbits were opened for perfusion following a published protocol [21]. Firstly, 100 ml pre-warmed 10 % formalin was injected into the abdominal aorta to fix the femoral vein. Then a confected radiopaque silicone rubber mix (MV-Diluent: MV-117 Orange: MV Curing Agent = 38: 47.5: 4.5) (Mirco-fil, Flow Tech Inc, USA) (http://www.flowtech-inc.com/products/) was perfused slowly into the vasculature of femurs. Subsequently, the animals were euthanized and stored at 4 °C overnight for complete polymerization of the in vivo-injected micro-fil. Finally, the bilateral femurs were separated and fixed in 10 % formalin, and then prepared for decalcification using 10 % ethylene diamine tetra-acetic acid (EDTA) decalcifying-fluid (AR1071, Boster, Pleasanton, CA, USA). EDTA was refreshed weekly, and the level of decalcification was assessed radiographically to confirm whether the samples were completely decalcified. The decalcified femur shaft was scanned by μCT using for imaging the perfused vessels with micro-fil. To segregate the infused radiopaque substance from the background, an Al1.0 filter was used, and the perfused micro-fil was defined at a threshold of more than 90 HU. The middle cortical bone (2 cm) of the femur shaft was selected as ROI, and then the 3D structure of blood vessels perfused by micro-fil were reconstructed and analyzed using a CT-Analyzer. The volume, number, and distribution of perfused micro-fil were measured.

2.4. Sequential fluorescence labeling of bone remodeling

A double-labeling procedure was performed to measure the dynamic bone formation. Xylenol orange (90 mg/kg body weight, 52097, Sigma–Aldrich) and calcein green (10 mg/kg body weight, C0875, Sigma–Aldrich) were injected subcutaneously on days 14 and 4 before euthanasia. Then, the femurs were collected and fixed in 10 % formalin for 1 week. After dehydration, the femur shaft was soaked in water-free methyl methacrylate (MMA, P107082, Aladdin) solution in gradient (MMA I, MMA II, and MMA III in sequence). Then, the femur shaft was embedded with MMA III solution without decalcification. Then the MMA-embedded samples were cut along the coronal plane and the transverse plane using a saw microtome (Exakt 300CP, Exakt Technologies. Inc., Basking Ridge, NJ, USA), respectively. And the sections were polished to 100-μm-thick using a polisher (Phoenix 4000, Buehler Ltd. USA) to observe fluorescence labeling. The undecalcified fluorescence labeling images were captured using a microscope (Leica DMI8, Leica Microsystems, Wetzlar, Germany). Histomorphometric analysis was carried out using the Image Pro-Plus 6.0 system (Version 6.0, Media Cybernetics. Inc., Rockville, MD, USA) and analyzed according to a standard histomorphometry protocol [28].

2.5. Histopathology

After euthanasia, the excised femora were fixed and decalcified using the same protocol as that used for angiographic architecture evaluation. After decalcification, the femur shaft was embedded in paraffin and cut into 5-μm-thick sections along the coronal plane and the transverse plane, respectively. The femoral diaphyseal cross sections and longitudinal sections were stained with hematoxylin and eosin (H&E, DH0006, League) for routine histology and tartrate resistant acid phosphatase (TRAP) dye (JoyTech Bio Co. Ltd., Zhejiang, China) for osteoclast identification. H&E and TRAP staining images were captured using digital whole-slide scanner (3DHISTECH, Pannoramic SCAN II, Hungary) and the histomorphometry was analyzed by 3DHISTECH's CaseViewer.

2.6. Immunohistochemistry and immunofluorescence

The decalcified femur shaft was embedded in paraffin and cut into 5-μm-thick sections along the coronal plane. Immunohistochemistry and immunofluorescence staining were performed according to the standard protocol. 1) Immunohistochemistry staining: Briefly, the sections were incubated with primary antibodies against goat leptin receptor (LepR, Abcam, ab50424, 1:200) overnight at 4 °C. The sections were then incubated with HRP-conjugated secondary antibodies to donkey anti-goat IgG H&L (Abcam, ab6885, 1:2000). Then sections incubated with 3, 3-diaminobenzidine tetrahydrochloride (DAB, Abcam, ab64238) for visualization. Nuclei were counterstained with hematoxylin. And then the images were observed by Leica DMi8 microscope (Leica, Wetzlar, Germany). The LepR + cells areas were quantified by Image-Pro Plus software (Version 6.0, Media Cybernetics. Inc., Rockville, MD, USA). 2) Immunofluorescence staining: Briefly, the sections were incubated with primary antibodies against rabbit periostin (Abcam, ab14041, 1:100), rabbit CD31 (Bioss, 0195R, 1:100), goat CGRP (Abcam, ab195387, 1:100) overnight at 4 °C. The sections were then incubated with fluorescence-conjugated secondary antibodies to goat anti-rabbit IgG H&L (Alexa Fluor®488) (Abcam, ab150081, 1:1000) and donkey anti-goat IgG H&L (Alexa Fluor® 594) (Abcam, ab150132, 1:1000). In the end, the sections were counterstained with DAPI (Boster, AR1177). The immunofluorescence images were captured using a research slide scanner (Olympus, VS200, Japan). And the fluorescence signals areas of Periostin, CD31, and CGRP were quantified by the Image Pro-Plus 6.0 system.

2.7. In vitro macrophages polarization assay

We further studied the effect of PDGF-BB on regulating the inflammatory response via balance the M1 and M2 types of macrophages. RAW 264.7 cells (5×10^3 cells/well) were cultured in 48-well plates with DMEM and incubated for 24 h. Then the cells were continued culture with medium containing 100 ng/ml LPS or 10 ng/ml IL-4 (Murine IL-4, PeproTech, 214-14) which all plus 10, 25, and 50 ng/ml PDGF-BB (Murine PDGF-BB, PeproTech, 315-18), 50 ng/ml VEGF (Murine VEGF156, PeproTech, 450-32) for another 12 h or 24 h. The CD86 (Biorbyt, ORB500820) and CD163 (Biorbyt, ORB182468) were used to evaluate the polarization of RAW 264.7 cells by immunofluorescence assay. The images were captured using a laser scanning confocal microscopy confocal (ZEISS, LSM900, Germany).

RAW 264.7 cells (10×10^4 cells/well) were cultured in 6-well plates with DMEM and incubated for 24 h. Then the cells were stimulated by LPS or IL-4 which all plus PDGF-BB for another 24 h or 48 h. The cells were washed and $0.5–1 \times 10^6$ cells were surface stained with FITC anti-mouse CD86 (BioLegend, 159220, 0.25 μg), PE anti-mouse CD80 (BioLegend, 104707, 0.5 μg), PE anti-mouse CD163 (BioLegend, 155308, 0.25 μg) for 1 h on ice. For intracellular CD206 staining, the cells were then fixed and permeabilized with Fixation/Permeabilization Buffer (eBioscience™, 00-5123-43) and stained with APC anti-mouse CD206

(BioLegend, 141708, 0.5 μg) for 1 h on ice. Then the polarization of RAW 264.7 cells were detected by Flow cytometry (EasyCell103A0, Shenzhen Wellgrow Technology Ltd. China), and the data were analyzed using Flowjo software (FlowJo, Ashland, OR, USA).

2.8. In vitro osteoclastogenesis assay

We further studied the effect of PDGF-BB on regulating osteoclast formation and function. RAW 264.7 cells (5×10^3 cells/well) were cultured in 48-well plates in the presence of 50 ng/ml murine sRANK ligand (RANKL, 315-11, PeproTech) plus 10, 25, and 50 ng/ml PDGF-BB, 50 ng/ml VEGF, and 156 ng/ml anti-PDGF-BB (rabbit PDGF-BB antibody, 500-P47, PeproTech) for 7 days. TRAP staining (#387, Sigma–Aldrich) was performed on day 4. TRAP-positive (TRAP+) multinucleated cells with more than three nuclei were counted as osteoclasts under a light microscope (Olympus, Tokyo, Japan). For measuring bone resorption function by pit formation assay, RAW 264.7 cells (3×10^3 cells/well) were seeded in Osteo Assay Surface 96-well multiple well plates (#3988, Corning) and cultured with RANKL (50 ng/ml) and drugs for 7 days, and the medium was changed every 3 days. On day 7, the cells on the plate were lysed with 4 % NaClO and the plate was washed with deionized water. The pit area in each plate was imaged using a dissecting microscope (Olympus, Tokyo, Japan). Quantification analysis was conducted in TRAP + multinucleated cells and pit areas using the Image Pro-Plus 6.0 system (version 6.0, Media Cybernetics. Inc, Rockville, MD, USA). Meanwhile, RAW 264.7 cells (2×10^4 cells/well) were cultured in 12-well plates in osteoclasts differentiation medium with PDGF-BB (10, 20 and 50 ng/ml), anti-PDGF-BB (156 ng/ml) for 2 days and 5 days, and the total protein was collected for analysis of osteoclast functions.

2.9. Quantitative (Real-time) PCR (qPCR)

RAW 264.7 cells (2×10^4 cells/well) were cultured in 12-well plates, the total RNA was extracted from the cells at 12 h after LPS or IL-4 stimulation, as well as RAW 264.7 at days 3, 5, and 7 after osteoclastogenesis induction, using the RNA Miniprep Kit (#AP-MN-RNA, Axygen®, Union City, CA, USA). Total RNA (200 ng) was reverse-transcribed to complementary deoxyribonucleic acid (cDNA) using the PrimeScript RT reagent kit (#RR036A, TaKaRa Biotechnology (Dalian) Co. Ltd, Dalian, China) with oligo dT primers and six random primers. The qPCR primers (BGI, Shenzhen, China) used in the experiments are listed in Table 1. The final reaction solution (20 μl) contained 1 μl of the diluted cDNA product, 10 μl of 2 × Power SYBR® Green PCR Master Mix (#RR820B, TaKaRa), 0.8 μl each of forward and reverse primers, and 7.4 μl nuclease-free water. The amplification conditions were as follows: 50 °C for 2 min, 95 °C for 10 min, 40 cycles of annealing at 95 °C for 15 s and annealing and extension at 60 °C for 1 min. The fluorescence signal was recorded using a Roche Light Cycler 480 Detection System (Germany) and converted into numerical values. The mRNA levels of all the genes were normalized using *gapdh* as an internal control. These analyses were performed in duplicates for each sample using cells from three different cultures, and each experiment was repeated three times.

2.10. Western blotting

Cells were lysed in RIPA lysis buffer containing 1 % PMSF and 1 % protease and phosphatase inhibitor cocktail (#78446, Thermo Fisher Scientific). After treatment on ice for 30 min, cell lysates were clarified by centrifugation at 12,000×*g* for 15 min at 4 °C to remove cell debris, and the protein content was measured using the Pierce™ BCA protein assay kit (#23227, Thermo Scientific™). The total lysates were boiled in 2 % sodium dodecyl sulfate polyacrylamide gel electrophoresis (SDS-PAGE) buffer. Aliquots of the lysates were subjected to 10 % SDS-PAGE (with 5 % stacking gel) and transferred to a PVDF membrane (#1620177, Bio-Rad Laboratories, Hercules, CA, USA). Immunoblotting was performed using primary antibodies to rabbit IL-1β (Novus, NB600-633, 1:2000), rabbit TGF-β (Youpin, YP-Ab-04780, 1:1000), rabbit Periostin (Abcam, ab14041, 1:2000), mouse VEGFA (Abcam, Ab28775, 1:2000), rabbit Netrin-1 (Abcam, Ab126729, 1:2000), rabbit CTHRC1 (LifeSpan BioSciences, LS-B10953, 1:2000), overnight at 4 °C. The PVDF membrane was then washed three times with Tris-buffered saline Tween (TBST) buffer solution (#37571, Thermo Scientific™) three times. Then, the membrane was incubated with HRP-conjugated secondary antibodies at room temperature for 2 h, and washed three times by TBST buffer solution. Protein bands were developed using an enhanced chemiluminescence detection kit (Multi Sciences Biotech Co. Ltd., Hangzhou, China), and band densities were quantified using Image Lab™ (Bio-Rad Laboratories) by calculating the average optical density in each field. The GAPDH antibody (Abcam, ab8245, 1:5000) was used as a reference to normalize the differences in the amounts of protein among samples.

2.11. Statistics

The difference in incidence and size of ON lesion in the cortical bone of each group, and the size of necrotic bone marrow were calculated and analyzed by the chi-square test. The μCT data, histological quantitative data and *in vitro* tests data were expressed as mean ± SEM, and analyzed by One-way ANOVA (Fisher-LSD) at a single time point for multiple comparisons. Statistical significance was set at $p < 0.05$. All statistical analysis was performed using the GraphPad Prism 8 software (GraphPad Software Inc., San Diego, CA, USA).

Table 1
Primer sequences used for real-time PCR.

Gene	Forward primer#	Reverse primer
M[a]-*Gapdh*	5′-CATGTTCCAGTATGACTCCACTC-3′	5′-GGCCTCACCCCATTTGATGT-3′
M-*IL-1β*	5′-GCAACTGTTCCTGAACTCAACT-3′	5′-ATCTTTTGGGGTCCGTCAACT-3′
M-*IL-6*	5′-TAGTCCTTCCTACCCCAATTTCC-3′	5′-TTGGTCCTTAGCCACTCCTTC-3′
M-*Mcp-1*	5′-TTAAAAACCTGGATCGGAACCAA-3′	5′-GCATTAGCTTCAGATTTACGGGT-3′
M-*Arg-1*	5′-CTGGCAGTTGGAAGCATCTCT-3′	5′-GTGAGCATCCACCCAAATGAC-3′
M-*IL-10*	5′-CTTACTGACTGGCATGAGGATCA-3′	5′-GCAGCTCTAGGAGCATGTGG-3′
M-*Tgf-β*	5′-CCACCTGCAAGACCATCGAC-3′	5′-CTGGCGAGCCTTAGTTTGGAC-3′
M-*Trap*	5′-GATGCCAGCGACAAGAGGTT-3′	5′-CATACCAGGGGATGTTGCGAA-3′
M-*Mmp9*	5′-CTGGACAGCCAGACACTAAAG-3′	5′-CTCGCGGCAAGTCTTCAGAG-3′
M-*Ctk*	5′-GAAGAAGACTCACCAGAAGCAG-3′	5′-TCCAGGTTATGGGCAGAGATT-3′

[a] M, *Mus musculus*; *Gapdh*, glyceraldehyde-3-phosphate dehydrogenase; *IL-6*, interleukin 6; *Mcp-1*, monocyte chemotactic protein 1; *IL-1β*, interleukin 1*β*; *Arg-1*, arginase 1; *IL-10*, interleukin 10; *Tgf-β*, transforming growth factor β; *Trap*, tartrated resistant acid phosphates; *Mmp9*, matrix metallopeptidase 9; *Ctk*, Cathepsin K. # Primers were synthesized by BGI (Shenzhen, China).

3. Results

3.1. The pathological characteristics of on lesion in the femoral diaphysis under SAON condition

In this study, we established a SAON model in rabbits using repeated intravenous injections of low-dose LPS (10 μg/kg) and followed by three intramuscular injections of high-dose MPS (20 mg/kg) at week 0 and week 2 (Fig. 1A). To evaluate the vascular changes in the femoral diaphysis, we collected femur samples and performed the μCT-based angiography at 6 weeks post-SAON induction.

In the normal group, the vascular network exhibited a well-organized architecture with fine branching. In contrast, the SAON group showed a disrupted vascular network, with small-sized angiographic agents lacking vessel-like architectural features, appearing denser and randomly oriented (Fig. 1B). Quantitative analysis of μCT-based angiography revealed an increase in the surface area and number of perfused substances ($p < 0.5$, SAON group vs. normal group), but no significant change in total volume. Notably, the proportion of small-sized (<200 μm) perfused substances increased in the SAON group, indicating sever vascular leakage compared to the normal group (Fig. 1C1–3). The histopathological examination of blood vessels further revealed inflammatory changes in the artery vascular endothelium, including hyperplasia and thickening, while vein venous walls exhibited partial fragmentation with endothelial cell pyknosis and karyorrhexis in the SAON group (Fig. 1D). These pathological changes in the vessel wall were consistent with the clinical features observed in human studies [29,30], confirming the presence of vasculitis. In certain areas of the lesion bone marrow, vessels exhibited venous stasis and necrosis, preventing the perfusion of micro-fil substances during angiography. Consequently, the surrounding fatty tissue, stem cells niche, and hemopoietic system were severely impaired.

Osteonecrosis (ON) was identified by the presence of diffusely empty lacunae or pyknotic nuclei of osteocytes [21]. In this study, ON and adjacent bone marrow lesions occurred synchronously due to ischemia secondary to SAON induction. Histopathological images of normal femur revealed an active haversian system, analogous to humans, with clearly distinguishable osteons, osteon fragment, and interstitial lamellae (Fig. 2A). Additionally, the normal marrow cavity was filled with stromal cells, fat cells, and blood vessels (Fig. 2B). In contrast, the SAON group exhibited extensive ON lesion in the cortical bone, with severe destruction of osteon and haversian canal structure. The adjacent bone marrow also displayed varying degrees of necrosis and lesions. Quantitative analysis results showed that ON lesion area (%Ct-Nec.Ar, %) occupied approximately 43.3 % (range: 7.0–81.7 %) of cortical bone area at 6 weeks post-SAON induction (Fig. 2C). Simultaneously, necrotic bone marrow tissue, characterized by necrotic fat, extended to 20.6 % (range: 4.2–45.4 %). The remaining lesion bone marrow tissue was replaced by fibrosis (Fibr.B.Ma, 36.6 %; range: 21.5–57.0 %), inflammatory infiltrates (Inflam.B.Ma, 33.1 %; range: 21.1–54.3 %), and sporadic newly formed bone tissue, identified as sclerotic areas (NFB.B.Ma, 4.2 %; range: 0.6–10.2 %) (Fig. 2D). Of note, perfused micro-fil substances were observed in inflammatory and sclerotic areas but were absent in necrotic bone marrow fat and fibrotic regions.

3.2. The alternations of osteogenic microenvironment in the femoral diaphysis under SAON condition

In addition to ischemia, the insufficiency of repair cells in the pathological condition of SAON is another disadvantage factor contributing to the slow process of new bone regeneration [20,31]. Leptin receptor (LepR) is a key marker of highly enriched MSCs, the LepR-positive (LepR+) cells are the primary source of osteoprogenitors for bone regeneration and remodeling in adult bone tissue [32]. In this study, the immunohistochemical staining revealed abundant LepR + cells in the normal cortical bone and bone marrow. In contrast, significantly fewer LepR + cells were observed in the necrotic cortical bone and lesioned bone marrow regions in the group (Fig. 3A). To further assess changes in the bone osteogenic microenvironment of the cortical bone under SAON condition, we analyzed the levels of periostin in the periosteum, as well as CD31 and CGRP in the femur shaft by immunofluorescence staining. Results showed significantly lower periostin level in periosteum regions adjacent to necrotic cortical bone (Nec.B), but higher perisotin in regions adjacent to non-necrotic cortical bone (Nor.B) in the SAON group (Fig. 3B). Within the center zone of Nec.B, the CD31 and CGRP levels markedly reduced compared to the normal cortical bone zone, indicating impairment of loss of intraosseous CD31-marked vessels and CGRP-marked nerves (Fig. 3C&D). However, in the SAON group, the CD31 and CGRP levels were significantly higher in or around the Nor.B zone compared to the Nec.B zone. Then, we further analyzed the CD31 and CGRP levels in the bone marrow tissue (Fig. 3C&D). As described in Section of 3.2 and Fig. 2B, we defined inflammatory and sclerotic areas (where micro-fil substances could be perfused) as repair reaction regions (Repair), and necrotic bone marrow fat and fibrotic areas (without micro-fil substances) as lesion regions (Lesion). Compared to normal bone marrow tissue, the lesion zones exhibited significantly lower CD31 and CGRP levels. In contrast, the repair reaction zones showed much higher CD31 and CGRP levels relative to the lesion zone in the SAON group. Notably, the CD31 and CGRP levels were also markedly increased in the repair reaction zone of the SAON group compared to the normal group.

3.3. PDGF-BB protects cortical bone in the femoral diaphysis under SAON condition

Analysis of GEO data (GSE123568) revealed lower PDGF-BB expression in peripheral blood mononuclear cells of SAON patients compared to non-SAON patients (Fig. S1). Consistent with this, our previous study demonstrated significantly higher PDGF-BB level in reparative osteogenesis area than in destructive repair area of SAON [21]. Based on these findings, we evaluated the potential of rhPDGF-BB (1 μg/dose or 2 μg/dose) on protecting cortical bone by injection into bone marrow cavity of proximal femur under SAON condition (Fig. 4A).

Firstly, we found PDGF-BB treatment stabilized the vascular network architecture and improved blood supply in the femur shaft (Fig. 4B). Quantitive analysis of μCT-based angiography showed a significant reduction in small-sized perfused substances (<400 μm) lacking vessel-like architectural features in the 2 μg/dose PDGF-BB-treated group compared to the SAON group (Fig. 4C). Additionally, the total surface areas and number of perfused substances decreased and trended toward baseline values in the 2 μg/dose PDGF-BB group. These results suggested PDGF-BB could protect primary blood vessels from SAON-induced damage. In addition, we further examined alterations in the 3D geometry of the femur shaft at 6 weeks post-SAON induction. Visual assessment revealed apparent differences in cortical bone geometry among the groups (Fig. 4D). Quantitative 3D analysis demonstrated that SAON group had significant lower values for T.Ar, B.Ar, Ps.Pm, Es.Pm and Rm compared to the normal group (Fig. 4E). However, the vBMD of cortical bone showed no difference between the normal and SAON groups (Fig. 4F). Of note, the biomechanical related markers, including pMOI and SSI, were both reduced by approximately one-third in the SAON group compared to the normal group (Fig. 4G&H). While treatment with 2 μg/dose PDGF-BB significantly restored the 3D geometry of the femur shaft under SAON condition. Structure and biomechanical parameters of cortical bone, including T.Ar, B.Ar, Ps.Pm, Es.Pm, Rm, pMOI and SSI, were recovered and trended toward normal levels compared the SAON group (Fig. 4E–H).

Collectively, these findings demonstrate that PDGF-BB treatment maintains the 3D geometry and biomechanical integrity of the femur shaft cortical bone under SAON conditions, highlighting its potential as a therapeutic agent to mitigate SAON-induced bone damage.

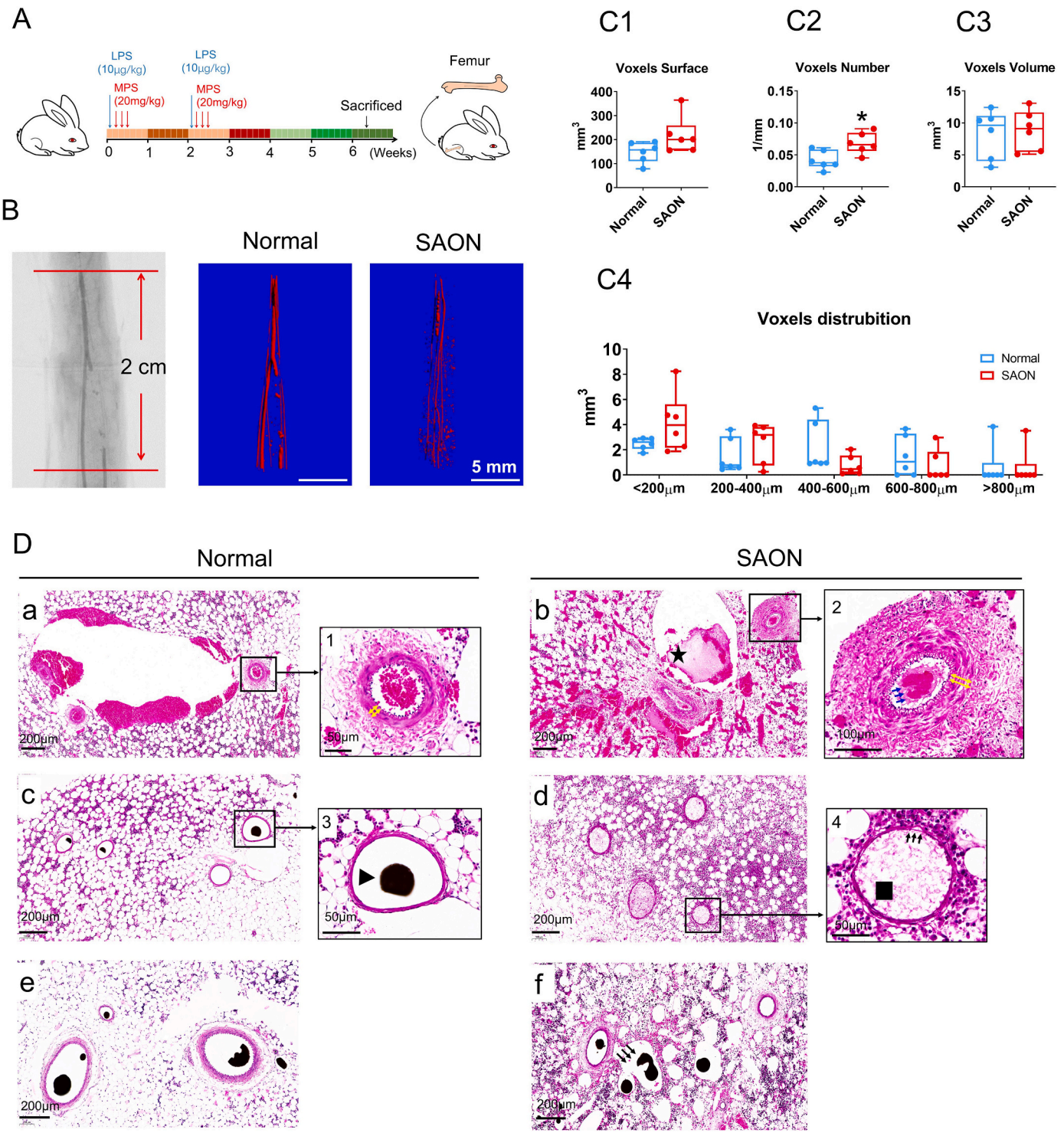

Fig. 1. The blood vessels in the femoral diaphysis were impaired in rabbits with SAON. (A) The SAON induction protocol. (B) The X-ray angiography image in normal femur mid-shaft was used to show the 2 cm region of interest (ROI) for 3D voxel analysis, and the representative 3D reconstructed voxels images in two groups (bar = 5 mm). (C) Quantitative analysis of Voxels surface (C1), Voxels number (C2), Voxels volume (C3), and the different sized voxels in two groups (C4), n = 6. The data were presented by grouped summary values with individual rabbit plotted as solid dots and analyzed by the independent sample t-tests (α = 0.05) for comparison to the normal group (*$p < 0.05$). (D) Representative H&E staining images showed the change of blood vessels in the bone marrow cavity of femur. Figure **a** showed the normal bone marrow tissue in the normal group, and Figure **b** showed the lesioned bone marrow tissue in the SAON group (bar = 200 μm). The normal vessels (**a1**, bar = 50 μm) and the lesioned vessels (**b2**, bar = 100 μm) which were the magnified images within the black boxes in **a** and **b**, the double yellow arrows showed the thickness of vascular endothelium, and the blue arrow showed the thrombosis within the affected vessel. The lesioned hemopoietic system was marked by ★. Figure **c** and **d** showed the bone marrow tissues post-perfused by micro-fil angiography (bar = 200 μm). The perfused substance inside the normal blood vessels (**c3**, bar = 50 μm) and the necrotic vessels without perfused substance (**d4**, bar = 50 μm), which were the magnified images within the black boxes in **c** and **d**. The perused substance was marked by ▲; The intravascular substance within the necrotic vessel was marked by ■. Figure **e** showed the perfused substance inside the normal blood vessels in the normal bone marrow tissue areas (bar = 200 μm). Figure **f** showed the damaged blood vessels (the black arrows) in the lesion of bone marrow tissue areas (bar = 200 μm).

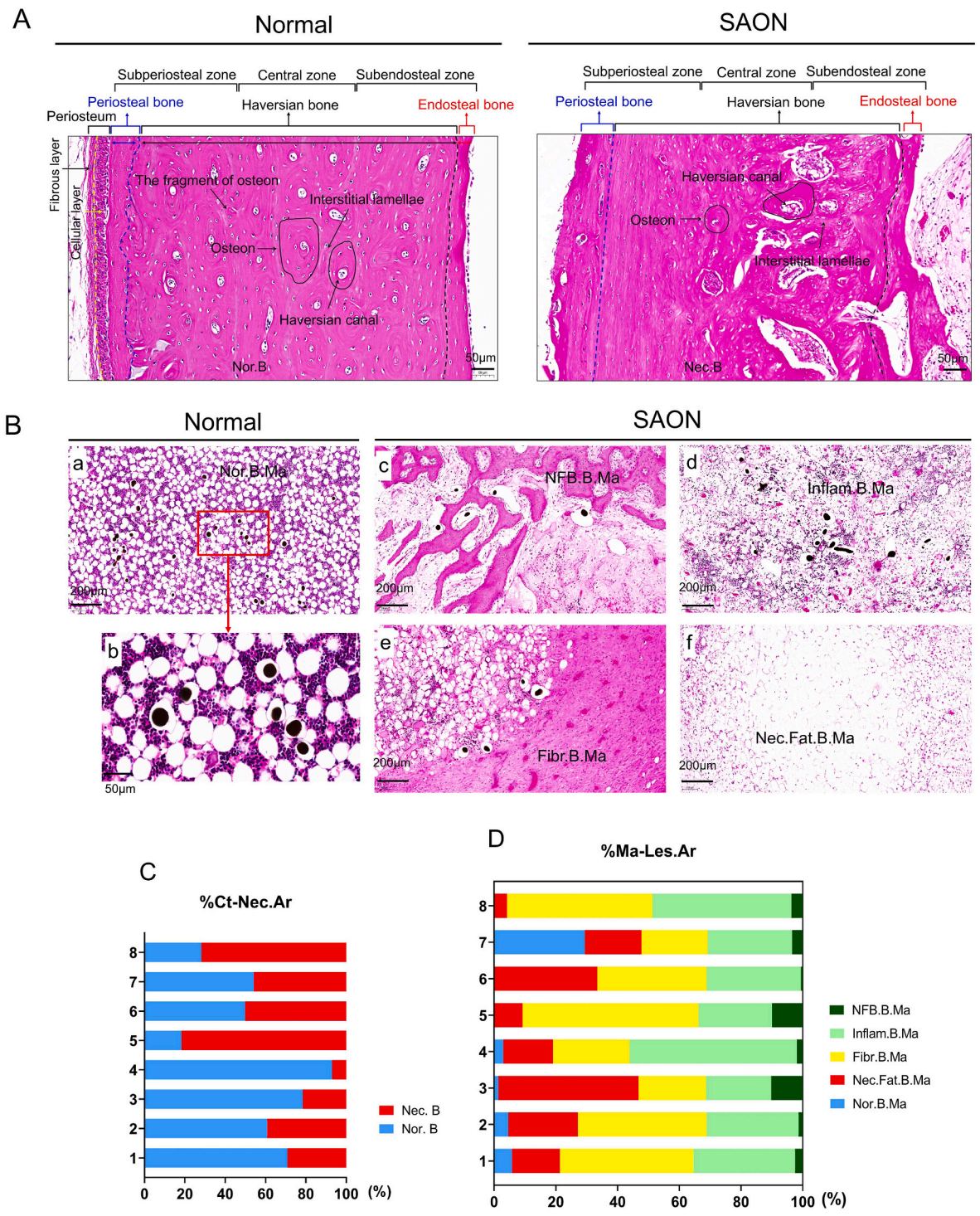

Fig. 2. The pathological characteristics of SAON lesion in cortical bone and bone marrow in the femoral diaphysis. (**A**) The alterations of histological microstructure of cortical bone in femur shaft post-SAON induction. The femoral diaphyseal cross sections were stained with H&E in normal and SAON rabbits, respectively (Bar = 50 μm). (**B**) The main pathological features of the normal or lesioned bone marrow tissue post-perfused by micro-fil angiography (**a**, **c-f**, bar = 200 μm; **b**, bar = 50 μm). Figure **a** and **b** showed the distribution of perfused substances in the normal bone marrow tissue areas. Figure **c** and **d** showed there were a lot of perfused substances into the newly formed bone tissue (**c**, NFB.B.Ma) and into those inflammatory tissue of bone marrow areas (**d**, Inflam.B.Ma). Figure **e** and **f** showed there were no perfused substances that could be observed in those fibrosis tissue (**e**, Fibr.B.Ma) and necrotic fatty tissues in the bone marrow areas (**f**, Nec.Fat.B.Ma). (**C-D**) Histomorphometry results based on longitudinal sections with H&E staining about the individual femur in SAON group (n = 8), and showed the ratio of necrotic cortical bone areas (**C**, %Ct-Nec.Ar) and the quantitative analysis of the lesion of bone marrow tissue areas (**D**, %Ma-Les.Ar) referring to the ratio of Nor.B.Ma, Nec.Fat.B.Ma, Inflam.B.Ma, Fibr.B.Ma, and NFB.B.Ma, respectively.

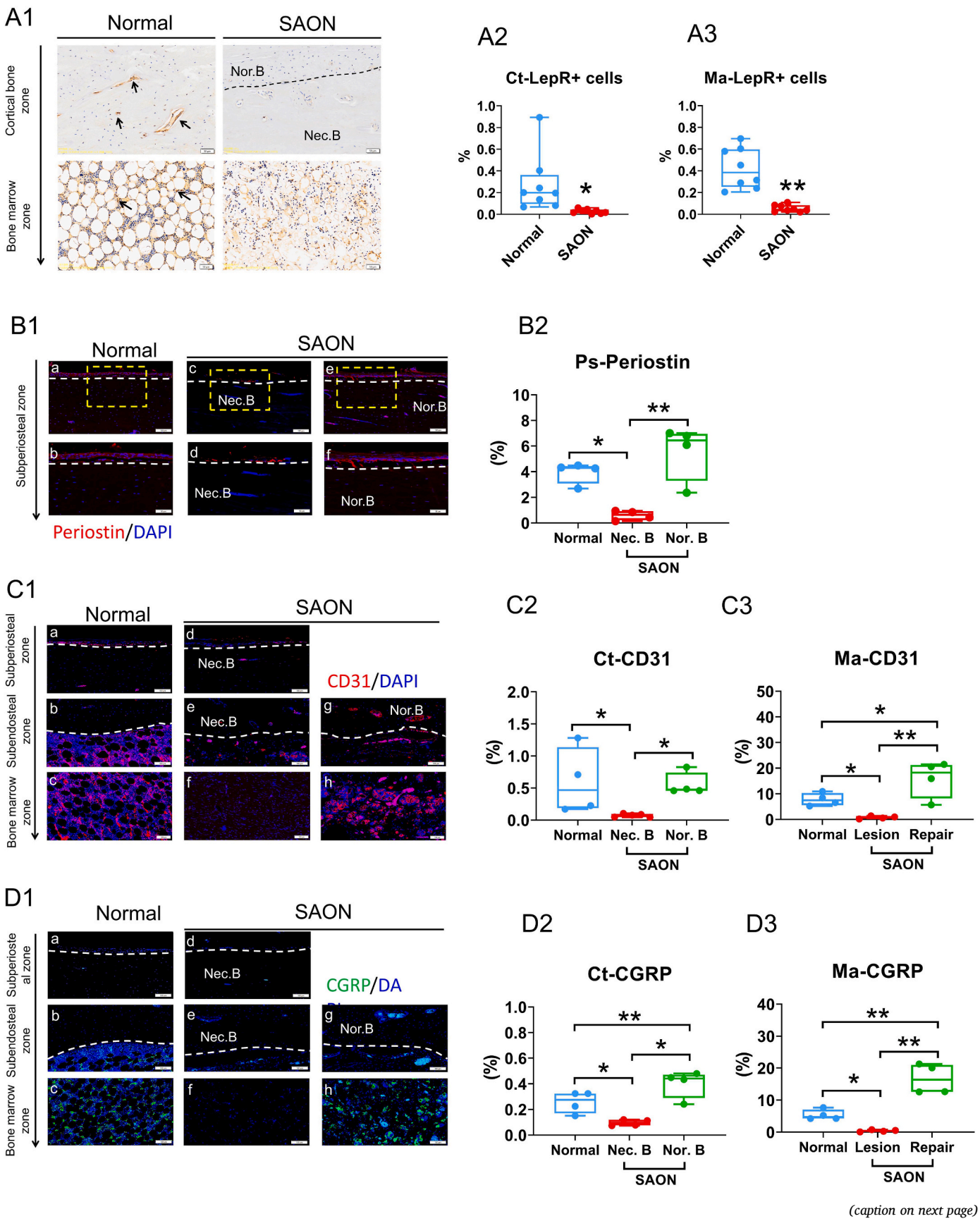

(caption on next page)

Fig. 3. The alterations of cortical bone osteogenic microenvironment in the femoral diaphysis post-SAON induction. (**A1**) Representative immunohistochemical staining images of LepR positive (LepR+) cells (black arrows) in the normal cortical bone and bone marrow areas with high intensity of LepR staining, and the necrotic bone and the fibrotic bone marrow tissues with low intensity of LepR staining (bar = 50 μm). (**A2-A3**) Quantification of LepR expressions within the cortical bone region (**A2**, Ct-LepR + cells, %) and bone marrow region (**A3**, Ma-LepR + cells, %). n = 8. $^{*}p < 0.05$, $^{**}p < 0.01$, independent sample t-tests ($\alpha = 0.05$) were employed for comparison to normal group in Fig. A. (**B1**) Representative immunofluorescence staining of periostin (red) images (bar = 100 μm). Figure **b**, **d**, and **f** showed the magnified areas (bar = 50 μm) within the yellow boxes in Figure **a**, **c** and **e**, respectively. (**B2**) Quantification of periostin expressions within the periosteum region (Ps-Periostin). n = 4. (**C1**) Representative immunofluorescence staining of CD31 (red) images based on the femoral diaphyseal longitudinal sections (bar = 100 μm). Figure **a** and **d** showed the subperiosteal zone; Figure **b**, **e**, and **g** showed the subendosteal zone; Figure **c**, **f**, and **h** showed the bone marrow zone. Figure **d** and **e** showed the necrotic bone (Nec.B) zone and Figure **f** showed the lesioned bone marrow tissues, while Figure **g** showed the normal bone (Nor.B) zone and **h** showed repair reactive zone within those lesioned bone marrow tissue areas post-SAON induction. Quantification of CD31 expressions within cortical bone region (**C2**, Ct-CD31, %) and bone marrow region (**C3**, Ma-CD31, %). n = 4. (**D1**) Representative immunofluorescence staining of CGRP (green) images based on the femoral diaphyseal longitudinal sections (bar = 100 μm). Figure **a** and **d** showed the subperiosteal zone; Figure **b**, **e**, and **g** showed the subendosteal zone; Figure **c**, **f**, and **h** showed the bone marrow zone. Figure **d** and **e** showed the Nec.B zone and Figure **f** showed the lesioned bone marrow tissues, while Figure **g** showed the Nor.B areas and **h** showed repair reactive areas within those lesioned bone marrow tissue zones post-SAON induction. Quantification of CGRP expressions within the cortical bone zone (**D2**, Ct-CGRP, %) and bone marrow zone (**D3**, Ma-CGRP, %). n = 4. All data in Figure B, C, and D were presented by box plots with individual rabbits plotted as solid circles and analyzed by the One-way ANOVA (Fisher-LSD multiple comparisons) ($^{*}p < 0.05$, $^{**}p < 0.01$).

3.4. PDGF-BB relieves the on progression in the femoral diaphysis under SAON condition

As described in Section 3.1, the ON in the femur shaft is accompanied by neighboring bone marrow lesion or necrosis. Of note, we found PDGF-BB treatment significantly alleviated ON pathologic progression in both cortical bone and bone marrow. This intervention reduced the incidence of ON from 100 % in the SAON group to 25–37.5 % (Fig. 5A&B). Histological analysis revealed that the micro-architecture of cortical bone and bone marrow, which had been damaged by SAON lesions, was restored following PDGF-BB treatment. Quantitative data demonstrated that the ON lesion areas in cortical bone was reduced to 9.1–16.5 % (Fig. 5C). Concurrently, the area of normal bone marrow increased to 86.3–88.8 % in PDGF-BB groups compared to the SAON group (Fig. 5D).

In addition, we further analyzed changes in the cortical bone microstructure. Histomorphometry analysis of cross-sections of femur shaft confirmed that the Osteon and the Haversian canal systems were severely damaged under SAON condition (Fig. 5E). In the SAON group, the Osteon density (Osteon.Dn, 1/mm^2) and the Haversian canal density (Ha.Ca.Dn, 1/mm^2) were significantly decreased, while the ratio of total Haversian canal area to cortical area (%Ha.Ca.Ar, %) was significantly increased compared to the normal group. However, no significant differences were observed in the ratios of total osteon area, total fragments of osteon area (% Frag.Osteon.Ar, %), and total interstitial lamellae area (% Inter.La.Ar, %) to cortical area. Histomorphometry analysis of longitudinal-sections further confirmed alterations in the canal system, consistent with changes in the Haversian canal system in cross-section. Specifically, the canals density (Ca.Dn,/mm^2) was decreased, while the ratio of total canals areas to cortical area (%Ct-Pore.Ar, %) was increased in the SAON group compared to the normal group (Fig. S2A). Of note, PDGF-BB treatment at 1 μg/dose or 2 μg/dose significantly restored cortical bone microstructure. The key parameters, referring to Ha.Ca.Dn, %Ha.Ca.Ar, Ca.Ar, %Ca.Ar, and % Frag. Osteon, were all recovered after PDGF-BB treatment. However, the % Inter. La. Ar was significantly increased in the 1 μg/dose PDGF-BB group compared to SAON group.

3.5. PDGF-BB accelerates cortical bone remodeling in the femoral diaphysis under SAON condition

The alterations in histological architecture parameters implied that SAON-affected cortical bone exhibited high porosity, which was associated with an imbalance between bone formation and resorption. The dual-fluorescent labeling analysis revealed a significant reduction in dynamic bone formation rate in the SAON-affected cortical bone of femur shaft (Fig. 6A&B). Specifically, the mineral apposition rate (MAR, μm/day), mineralizing surface (MS/BS, %), and bone formation rate (BFR/BS, μm3/μm2/day) on periosteal surfaces of cortical bone, as well as MS/BS and BFR/BS on endosteal surfaces (Fig. 6C), were significantly lower in SAON group compared to normal group. Correspondingly, TRAP staining results showed a significantly increase in TRAP + osteoclast number (N.Oc/BS, 1/mm) and eroded surface (ES/BS, %) on the endosteal surfaces of cortical bone and the canals surfaces of intercortical bone in SAON group compared to normal group (Fig. 6D&E). And we observed a thinner periosteum (Ps.Th) in the peri-periosteal cortical bone under SAON condition. However, PDGF-BB treatment protected periosteum from SAON-induced damage (Fig. S2B). Of note, PDGF-BB treatment at 2 μg/dose maintained the dynamic bone formation rate at normal level in SAON group. The MAR and BFR/BS values on both periosteal or endosteal surfaces of cortical bone were similar to those in the normal group, but significantly higher than those in the SAON group (Fig. 6). Meanwhile, PDGF-BB treatment at 2 μg/dose significantly reduced osteoclasts formation (Ct-N.Oc/BS) and function (Ct-ES/BS; Es–ES/BS) on both canals surfaces and on endosteal surfaces of cortical bone compared to SAON group.

In contrast, PDGF-BB treatment at 1 μg/dose showed limited bone remodeling capacity. Specifically, the values of MS/BS, MAR, and BFR/BS on the periosteal or endosteal surfaces of cortical bone in the 1 μg/dose group showed no significant difference compared to the SAON group and were significantly lower in MAR and BFR/BS when compared to the 2 μg/dose PDGF-BB group (Fig. 6C). Furthermore, PDGF-BB treatment at 1 μg/dose increased the ratio of total interstitial lamellae area to cortical bone area (%Inter.La.Ar, %) (Fig. 5C7) and the Ca.Dn in the cortical bone zone (Fig. S2A), suggesting the presence of immature woven bone in the 1 μg/dose PDGF-BB group under SAON condition. Correspondingly, structure and biomechanical parameters of cortical bone (including B.Ar, Rm, pMOI and SSI) in 1 μg/dose PDGF-BB group were decline compared to 2 μg/dose PDGF-BB group (Fig. 4E–H). Collectively, PDGF-BB treatment at 2 μg/dose was superior to 1 μg/dose in improving cortical bone remodeling capacity, effectively restoring the balance between bone formation and resorption in the SAON-affected femur shaft.

3.6. PDGF-BB regulates macrophage activation and osteoclast function

It is well as known, the initial inflammatory phase is more important for the bone repair [33]. Macrophage polarization is central to this process, as they not only control inflammation response but also contribute to tissue repair through the release of growth factors and chemokines [34]. PDGF-BB has been demonstrated to play a pivotal role in the early inflammatory phase of bone healing [15]. Therefore, our study focused on investigating the polarization of RAW 26.7 macrophages *in vitro*. Considering the complex and diverse microenvironment *in vivo*, we analyzed the macrophage polarization and their functions by stimulation with either LPS alone or a combination LPS and IL-4 *in vitro*. LPS/IL-4 induced macrophages were identified as a homogeneous population exhibiting a mixture of the characteristics of M1 and M2

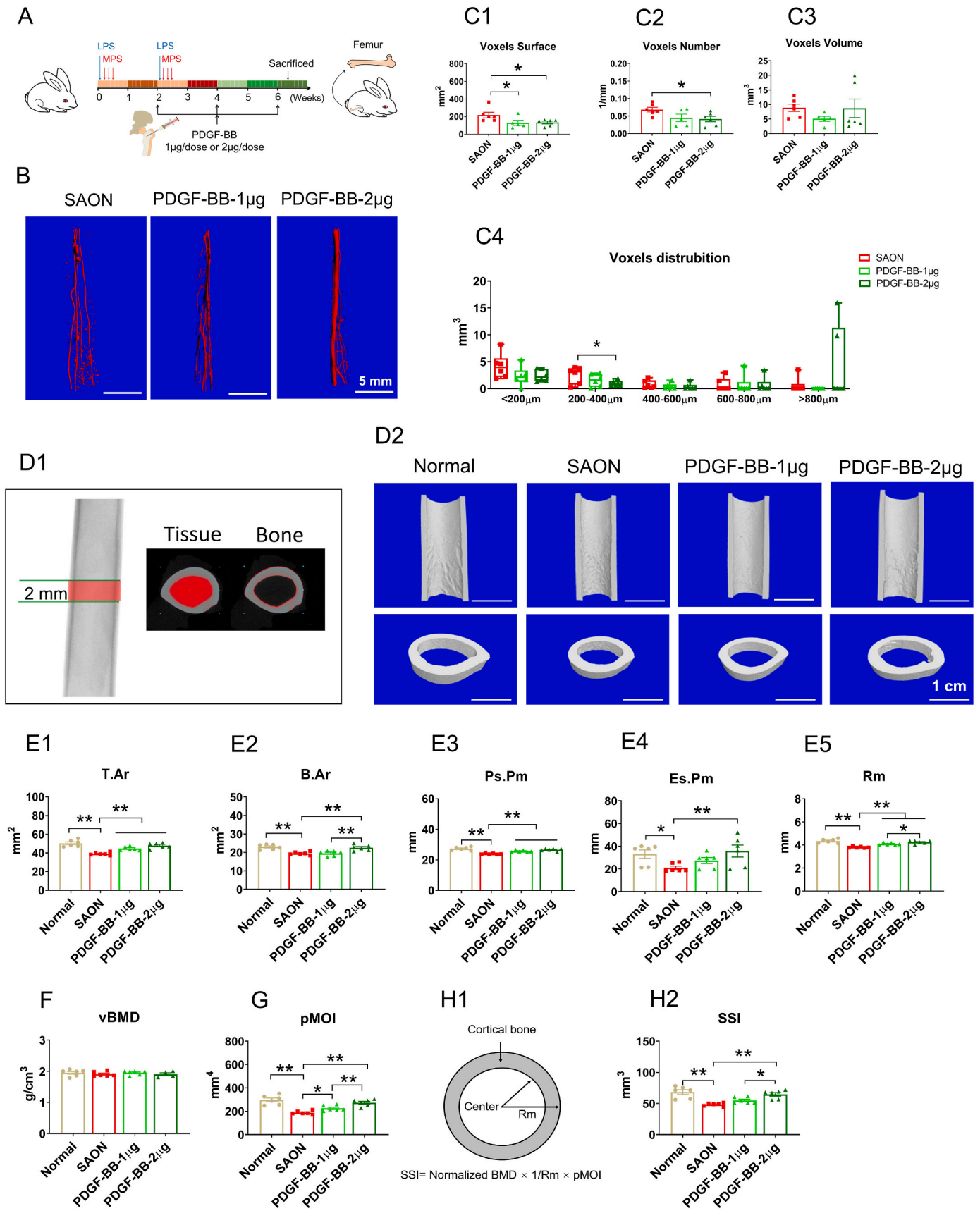

(caption on next page)

Fig. 4. PDGF-BB promotes the restoration of blood supply and cortical bone 3D architecture in the femoral diaphysis under SAON condition. (**A**) The PDGF-BB treatment protocol after SAON induction. (**B**) The representative 3D reconstructed voxels images in each group after PDGF-BB treatment (bar = 5 mm). (**C**) Quantitative analysis of Voxels surface (**C1**), Voxels number (**C2**), Voxels volume (**C3**), and the different sized voxels in the femur shaft in each group (**C4**), n = 6. (**D1**) The X-ray image was used to show the 2 mm ROI in the middle of femur shaft for 2D and 3D analysis. (**D2**) Representative 3D structure images of cortical bone in each group (bar = 1 cm). (**E**) Quantitative 2D analysis results showed Tissue areas (**E1**, T.Ar, mm^2) and Bone areas (**E2**, B.Ar, mm^2), Periosteum perimeter (**E3**, Ps. Pm, mm), Endosteum perimeter (**E4**, Es.Pm, mm), and Radius of cortical bone (**E5**, Rm, mm). (**F**) Quantitative 3D analysis results showed volumetric bone mineral density (vBMD, g/cm^3). (**G**) Quantitative 2D analysis results showed the mean polar moment of inertia (pMOI, mm^4). (**H1**) The calculation method of strength strain index (**H1**, SSI, mm^3) of cortical bone according to the CT values. SSI=Normalized vBMD × 1/Rm × pMOI. (**H2**) The SSI values in each group. n = 6. The data were presented by grouped summary values with individual rabbit plotted as solid dots and analyzed by the One-way ANOVA (Fisher-LSD multiple comparisons) (*$p < 0.05$, **$p < 0.01$).

macrophages [35].

As shown in Fig. 7, we first analyzed the populations of the CD86+ CD80+ M1-type macrophages and CD206 + CD163+ M2-type macrophages at 24 h post stimulation with LPS or LPS/IL-4 stimulations by flow cytometry, respectively. The analysis revealed that PDGF-BB significantly inhibited M1-type macrophages polarization while having no significant effect on M2-type macrophage polarization at 24 h post-stimulations (Fig. 7A&B, Fig. S4). However, at 48 h post-LPS/IL-4 stimulation, we observed a significant increase in CD163+ M2-type macrophages in PDGF-BB (10 and 50 ng/ml) groups compared to LPS/IL-4 control group (Fig. S5). Furthermore, the expression of CD86 was significantly decreased following PDGF-BB (10 and 25 ng/ml) treatment compared to LPS stimulation control group at 24 h post-stimulation (Fig. 7C). Conversely, the expression of CD163 at 24 h was significantly increased compared to LPS/IL-4 stimulation control group (Fig. 7D). To further investigate the molecular mechanisms, we assessed the mRNA levels of inflammatory markers in both macrophage types (Fig. 7E&F). In M1-type macrophages at 12 h post-LPS stimulation, we observed significantly reduced mRNA levels of *IL-1β* and *IL-6* in the PDGF-BB treatment groups (10 and 25 ng/ml). In M2-type macrophages at 12 h post-LPS/IL-4 stimulation, we found markedly increased mRNA levels of *TGF-β* in the PDGF-BB treatment groups. Correspondingly, the protein level of IL-1β in M1-type macrophages was also downregulated, while no significant increase in TGF-β protein level was observed in M2-type macrophages compared to control groups at 24 h post-stimulation (Fig. 7G). These findings collectively indicated that PDGF-BB modulates the inflammation response by suppressing the proinflammatory activity of M1-type macrophages in the early stage, while showing limited effect on M2-type macrophages function in an inflammatory setting.

Additionally, we further evaluated the effect of PDGF-BB on modulating osteoclasts activity (Fig. 8). TRAP staining (RANKL treatment for 4 days) and Pit assay (RANKL treatment for 7 days) revealed that VEGF (50 ng/ml) significantly increased the number of osteoclasts (N.Oc/Wells) and the area of resorption pits (Ar. Pit/Well) (Fig. 8A&B). Correspondingly, VEGF (50 ng/ml) upregulated the mRNA expressions of osteoclast marker genes (*Trap, Mmp-9, Cathepsin K)* were increased on days 3, 5 after RANKL induction compared to control group (Fig. S6). In contrast, the low dose of PDGF-BB (10 ng/ml) slowed osteoclast differentiation and reduced bone resorption activity when compared to both the high dose of PDGF-BB (50 ng/ml) group and control group (Fig. 8A&B). Consistent with these findings, the expression of osteoclast marker genes of *Trap* and *Cathepsin K* were markedly downregulated in the 10 ng/ml PDGF-BB group compared to the control group (Fig. 8C). However, no significant differences in these markers (*Trap, Mmp-9, Cathepsin K)* were observed between the 50 ng/ml PDGF-BB group and the control group during osteoclast differentiation and maturation (Fig. S6). Furthermore, the proliferation rate of RAW 264.7 cells was reduced in VEGF group at 2 days after RANKL-mediated osteoclast differentiation (Fig. 8D). In contrast, PDGF-BB (25 and 50 ng/ml) treatment did not affect RAW 264.7 cells proliferation or influence osteoclast formation at the end of the osteoclastic differentiation process. Additionally, anti-PDGF-BB (156 ng/ml) treatment inhibited osteoclast function by reducing osteoclastic marker genes.

With regard to the macrophage lineage TRAP + cells are known to provide could provide coupling signals that mediate new bone formation through multiple mechanisms [36]. For example, TRAP + cells secrete periostin, which can reconstruct the osteogenic microenvironment of the periosteum [17]; while TRAP + cells secrete VEGF and Netrin-1, which can target vascular endothelial cells and nerve cells, respectively, to induce vessels and nerve axonal growth [37]; furthermore, TRAP + cells express the collagen triple helix repeat containing 1 (CTHRC1), which assists osteoclasts in degrading the bone collagen matrix and releasing activated TGF-β, thereby targeting stromal cells and stimulating osteogenesis [38]. To explore this further, we measured the protein levels of Periostin, Netrin-1, VEGFA and CTHRC1 protein levels in TRAP + osteoclasts at days 3 and 5 after RANKL induction (Fig. 8E&F). The results indicated that 10, 25 and 50 ng/ml PDGF-BB significantly upregulated the Periostin, Netrin-1, VEGFA and CTHRC1 expressions during osteoclasts differentiation and maturation processes.

4. Discussion

In this study, we discovered for the first time that osteonecrotic lesion extended into the femoral diaphyseal regions and exhibited pathological characteristics of cortical bone in SAON rabbit model. This finding suggests that cortical bone degeneration in the femoral diaphysis may be associated with an increased risk of postoperative complications in case of SONFH. Concurrently, we proved that PDGF-BB treatment, administered via intramedullary injection into the femoral proximal marrow cavity at doses of 1 μg and 2 μg per dose, effectively remodeled necrotic cortical bone and regenerated damaged bone marrow tissue in the SAON affected femoral diaphysis. I*n vitro* biological analysis further revealed that PDGF-BB not only modulated M1-type macrophages transformation to reduce the inflammatory response, but also subsequently provided a secondary source of bioactivity factors (Periostin, Netrin-1, VEGFA, and CTHRC1) during osteoclast formation processes, thereby supporting sustained bone remodeling and improving cortical bone quality in SAON condition.

Microcirculation disturbance is one of the main pathogenic factors of SAON in patients undergoing high-dose/extensive GC use [30,39]. Previously, we reported that inadequate blood supply was caused by intravascular thrombus occlusion and extravascular marrow lipid deposition during early stage of SAON (at 2 weeks after LPS and MPS injection) [20,40]. However, at later stage (at 6 weeks after LPS and MPS injection), the primary blood supply was largely absent, and the surviving vessels presented severe leakage, ultimately leading to reduced blood perfusion and impaired venous return in the proximal femoral metaphysis and femoral head [20,41]. In this study, we also noticed that the arterial blood supply in the femoral diaphysis was also compromised, accompanied by inflammation and hyperplasia of the vascular endothelium. Additionally, venous blood flow appeared partially stagnant and even necrosis, with evidence of clear signs of vasculitis in SAON condition (at 6 weeks after LPS and MPS injection). In the context of vasculitis, the surrounding fatty tissue, stem cells niche, and hemopoietic system were impaired due to nutrient deficiencies and inflammatory responses. Recently, it has been reported that high-dose/short-duration GC use in patients with vasculitis accelerates aggressive SAON progression, accompanied by rapid bone destruction [6,29,42]. Indeed, in our SAON rabbit model at 6 weeks post-LPS and MPS injection, the affected femoral head exhibited active destructive

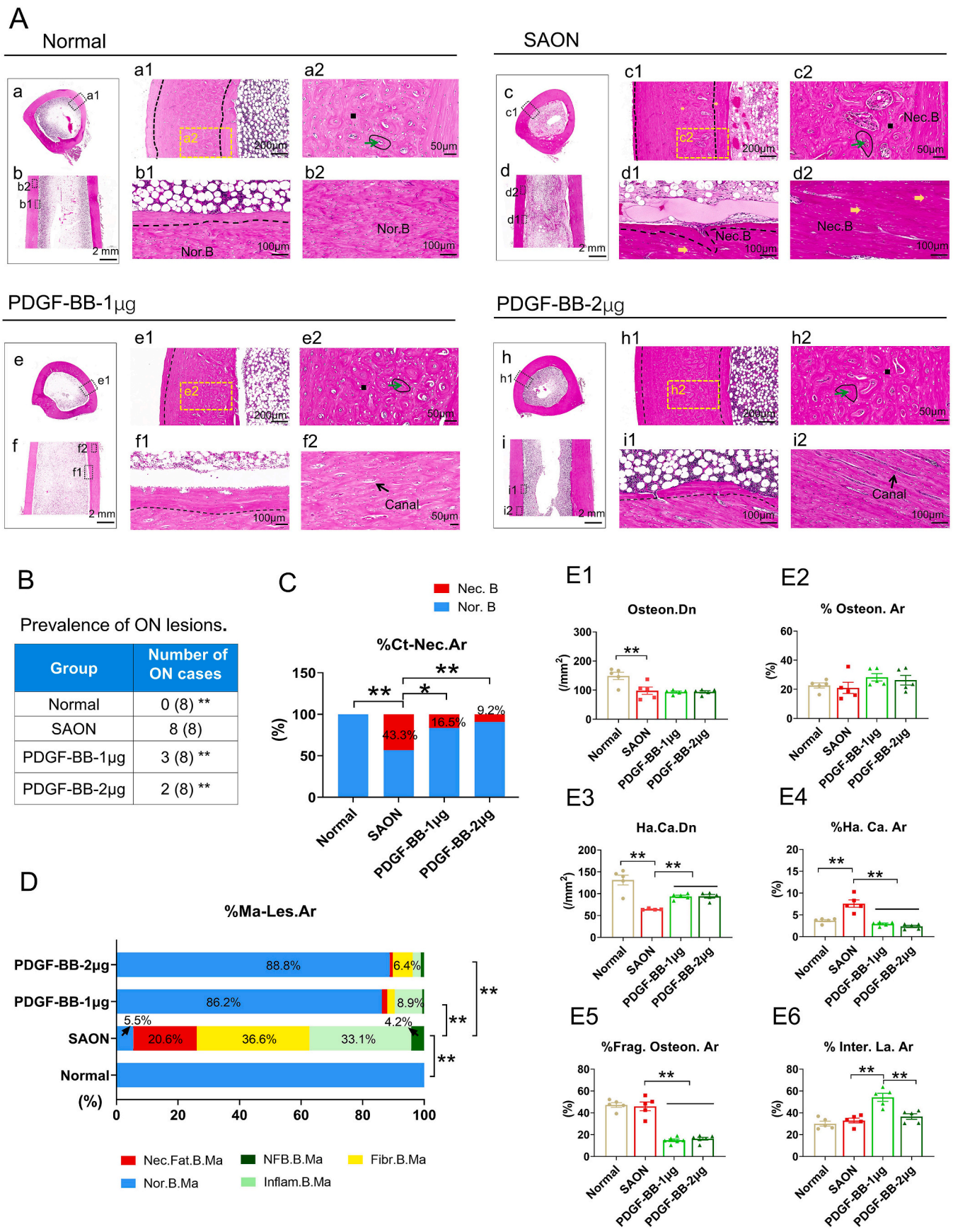

(caption on next page)

Fig. 5. PDGF-BB restores the cortical bone histological micro-architecture in the femoral diaphysis under SAON condition. (**A**) The femoral diaphyseal cross sections (**a**, **c**, **e**, **h**) and longitudinal sections (**b**, **d**, **f**, **i**) were stained with H&E in each group (bar = 2 mm), respectively. Figure a1, **a2**, **c1**, **c2**, **e1**, **e2**, **h1** and **h2** showed the magnified areas in cross sections, and Figure b1, **b2**, **d1**, **d2**, **f1**, **f2**, **i1** and **i2** showed the magnified areas in longitudinal sections. Yellow arrows showed necrotic bone (Nec.B); Black circles showed the Osteons; Green arrows showed the Haversian canals; Black arrows showed the canals; Solid black squares showed the interstitial lamellae. (**B**) The prevalence of ON lesions was examined by H&E staining at the end of this experiments. The data in Figure B were analyzed by the Chi-square test (**$p < 0.01$, compared to SAON group. n = 8). (**C-D**) Histomorphometry results based on longitudinal sections in each group, and showed the ratio of necrotic cortical bone areas (**C**, %Ct-Nec.Ar) and the quantitative analysis of the lesion of bone marrow tissue areas (**D**, %Ma-Les.Ar) referring to the ratio of Nor.B. Ma, Nec. Fat.B.Ma, Inflam.B.Ma, Fibr.B.Ma, and NFB.B.Ma, respectively. The data of %Ct-Nec.Ar, and %Ma-Les.Ar were presented by grouped summary values and analyzed by the Chi-square test (*$p < 0.05$, **$p < 0.01$, n = 8). (**E**) Histomorphometry results based on cross sections showing the osteon density (**E1**, Osteon.Dn,/mm^2), the ratio of total osteon areas to the cortical area (**E2**, % Osteon.Ar, %), the Haversian canals density (**E3**, Ha.Ca.Dn,/mm^2), the ratio of total harversian canals area to cortical area (**E4**, % Ha.Ca.Ar, %), the ratio of total fragments of osteon areas to the cortical area (**E5**, % Frag. Osteon. Ar, %), and the ratio of total interstitial lamellae area to cortical area (**E6**, % Inter. La. Ar, %). n = 5. The data in Figure E were presented by grouped summary values with individual rabbit plotted as solid dots and analyzed by the One-way ANOVA (Fisher-LSD multiple comparisons) (*$p < 0.05$, **$p < 0.01$).

repair but insufficient reparative osteogenesis, indicating rapid pathological progression [21,41]. Clinical imaging and histological evidence have shown that SAON not only involves the femoral head but may also extend into the neck, metaphyseal, and diaphyseal regions [12]. Herein, using the same SAON rabbit model, we observed that osteonecrotic lesions extended into the femoral diaphyseal regions, with necrotic lesion affecting approximately 43.3 % of the cortical bone and 94.5 % of the bone marrow tissue.

Correspondingly, the femur shaft geometry and the histological microarchitecture of the cortical bone were severely damaged. CT data revealed that structural parameters of the femur shaft, including T.Ar, B. Ar, Ps. Pm, Es. Pm and Rm of cortical bone, were all reduced, and mechanical markers such as pMOI and SSI also declined. Histological evidence further indicated that the Osteon and the Haversian canal systems of cortical bone were damaged in the osteonecrotic lesion regions, with an increase in %Ha.Ca.Ar and a decrease in Osteon.Dn. It has been reported that femur geometry determines tensile stress on the lateral cortex, and these pathological changes, combined with high mechanical stresses in the femur shaft, can lead to increased local microdamage and, ultimately, fracture [43,44]. In fact, the cortical bone 3D geometry and histoarchitecture can be corrected through bone modeling and remodeling in secondary bone healing process [45]. This process involves osteoclast-mediated resorption on the endosteal surfaces and periosteal apposition as an adaptive response to compensate for bone strength loss caused by age-related and chronic inflammatory disease-induced endosteal bone resorption [45]. If periosteal apposition increases, cortical bone strength can be maintained, conversely, if periosteal apposition decreases, endosteal resorption results in cortical bone weakening and thinning [46]. However, in the SAON affected femoral diaphysis, we observed numerous TRAP + multinuclear osteoclasts on the canals surface adjacent to the necrotic bone zone, but less LepR + MSCs contributing to bone regeneration. The periosteum layer near necrotic cortical bone regions became thinner, along with a reduction in periostin level. Of note, we also observed a decrease in CD31-marked intraosseous vessels and CGRP-marked sensory nerves in the central regions of the necrotic cortical bone. Collectivity, such alternations indicate the cortical bone remodeling environment is severely compromised under SAON condition.

GCs are known to inhibit osteoblast activity by obstructing cellular metabolism and inducing apoptosis, resulting in a suppression of the bone turnover rate [47]. In animal experiments involving high-dose/chronic administration of GCs to induce steroid associated osteoporosis (SAOP), a rapid decline in trabecular BMD at the proximal femur was observed, with subsequent recovery following discontinuation of GCs [48]. However, the thinning of the cortical shell in the femur shaft did no recover after the discontinuation of GCs, suggesting the cortical bone damage might be cumulative [49]. Moreover, in GCs-affected cortical bone, bone formation was almost completely suppressed [50]. Our previous study found that high-dose/short-duration GCs injection induced both SAON and SAOP in the same weight-bearing bone regions, such as femoral neck, those regions showed weakened cortical bone and decreased trabecular BMD [51]. A clinical study reported a high prevalence of SAOP in a large population of SAON patients, and with a 5-fold increased risk of SAOP in those who experienced fractures [52]. As recently reviewed, high dose/extensive GCs use is independently associated with an increased risk of atypical femoral fracture (AFF) [53]. Histological observation of AFF revealed that osteocytes in the fracture sites consisted mainly of empty lacunae, indicating the ON areas are susceptible to stress fracture [44]. In this study, we further observed extensive ON lesion and high porosity in the cortical bone of femur shaft in SAON condition, accompanied by decreased MAR, MS/BS and BFR/BS values both on periosteal and endosteal surfaces of the cortical bone. These findings help explain why 30 % of high dose GC users with subtrochanteric fracture experience atrophic non-union after surgical treatment, compared to 3–15 % in non-GC users [9,54]. In addition, subtrochanteric fractures require a long period of time for bone fusion, with an average duration was 8.3 months, while patients on high-dose GC use require even longer healing time, averaging 13 months [9,55]. Therefore, providing adjuvant therapies to restore the osteogenic microenvironment may help reduce the risk of complications (such as subtrochanteric fracture, loosening, periprosthetic fracture) following CD or THA surgical procedures in SONFH patients.

PDGF-BB as an "angiogenesis coupling osteogenesis" stimulatory protein combined with collagen and β-tricalcium phosphate has been commercialized for the treatment of bone defect and to facilitate bone fusion, particularly in patients who at high risk for non-union in lower extremity sites [13]. It has demonstrated similar fusion rates to autologous grafts with fewer adverse effects [56]. Preclinical studies have further showed that PDGF-BB can enhance the mechanical strength of tibial and femoral fractures in specific metabolic bone disease conditions, such as in geriatric osteoporosis and diabetes [57,58]. Our previous study proved that local injection PDGF-BB into proximal femur promoted angiogenesis and osteogenesis in the femoral head under SAON condition [21]. However, it remained unclear whether PDGF-BB could correspondingly improve cortical bone quality in the femoral diaphysis under the same setting. In this study, we observed the formation of a stable vascular network and sufficient blood supply in the femur following PDGF-BB treatment. Enhanced periosteal/endosteal osteogenesis along the cortical bone, as well as the renewal of damaged bone marrow tissue, were observed in those PDGF-BB-treated rabbits at 6 weeks post-SAON induction. CT-based cortical bone structure and mechanic parameters (T.Ar, B. Ar, Ps. Pm, Es. Pm, Rm, pMOI and SSI) all improved, and trending toward normal baseline values. Histological observation displayed enhanced bone remodeling (increased MAR and BFR/BS values on both periosteal and endosteal surfaces) and reduced osteoclasts formation and function (decreased N.Oc/BS and ES/BS values on canals and on endosteal surfaces), characterized by improved Osteons and Haversian canal system. Finally, PDGF-BB treatment reduced ON area to 9.1 %–16.5 % of the cortical bone and renewed neighboring bone marrow, with normal areas within the marrow cavity increasing to 86.2–88.8 % in the SAON-affected femoral diaphysis.

In fact, chronic inflammation is a hallmark of SAON, and rapid bone destruction is closely related to abundance of macrophages infiltration

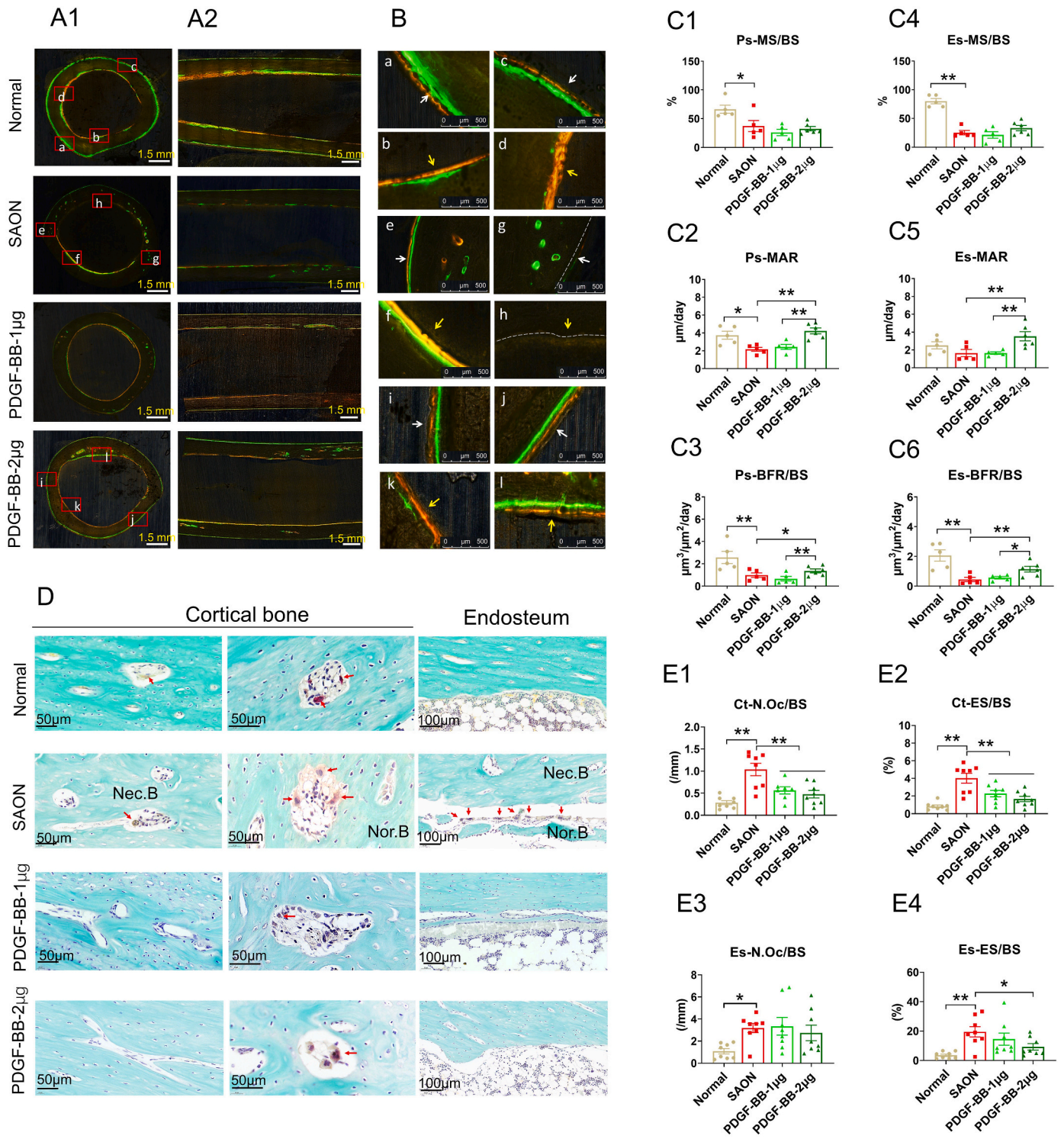

Fig. 6. PDGF-BB enhances cortical bone remodeling in the femoral diaphysis under SAON condition. (**A**) Dual-fluorescent micrographs of the un-decalcified cross (**A1**) and longitudinal (**A2**) sections of cortical bone at femur mid-shaft, the newly formed bone was labeled by Calcein green and Xylenol orange (bar = 1.5 mm). (**B**) The magnified areas within the red boxes in **A1** (bar = 500 μm). Figure **a**, **b**, **c** and **d** showed the magnified areas within the red boxes in Normal group, Figure **e**, **f**, **g**, and **h** showed the magnified areas within the red boxes in SAON group, and Figure **i**, **j**, **k**, and **l** showed the magnified areas within the red boxes in PDGF-BB-2 μg group, respectively. White arrows showed the periosteal surfaces; Yellow arrows showed the endosteal surfaces. (**C**) Histomorphometry results based on cross sections showing the mineral apposition rate (MAR, μm/day), mineralizing surface (MS/BS, %), and bone formation rate (BFR/BS, $\mu m^3/\mu m^2$/day) in periosteal (**C1-3**) and endosteal (**C4-6**) surfaces of cortical bone, respectively. n = 5. (**D**) The femoral diaphyseal longitudinal sections were stained with TRAP/Fast green staining. Red arrows showed osteoclasts. (**E1-4**) Histomorphometry results show TRAP + osteoclast number (N.Oc/BS, 1/mm) and eroded surface (ES/BS, %) on the surfaces of the canals within cortical bone zone (**E1-2**, Ct-) or on the endosteal surface (**E3-4**, Es-) respectively. n = 8. The data were in Figure C & E presented by grouped summary values with individual rabbit plotted as solid dots and analyzed by the One-way ANOVA (Fisher-LSD multiple comparisons) (*$p < 0.05$, **$p < 0.01$).

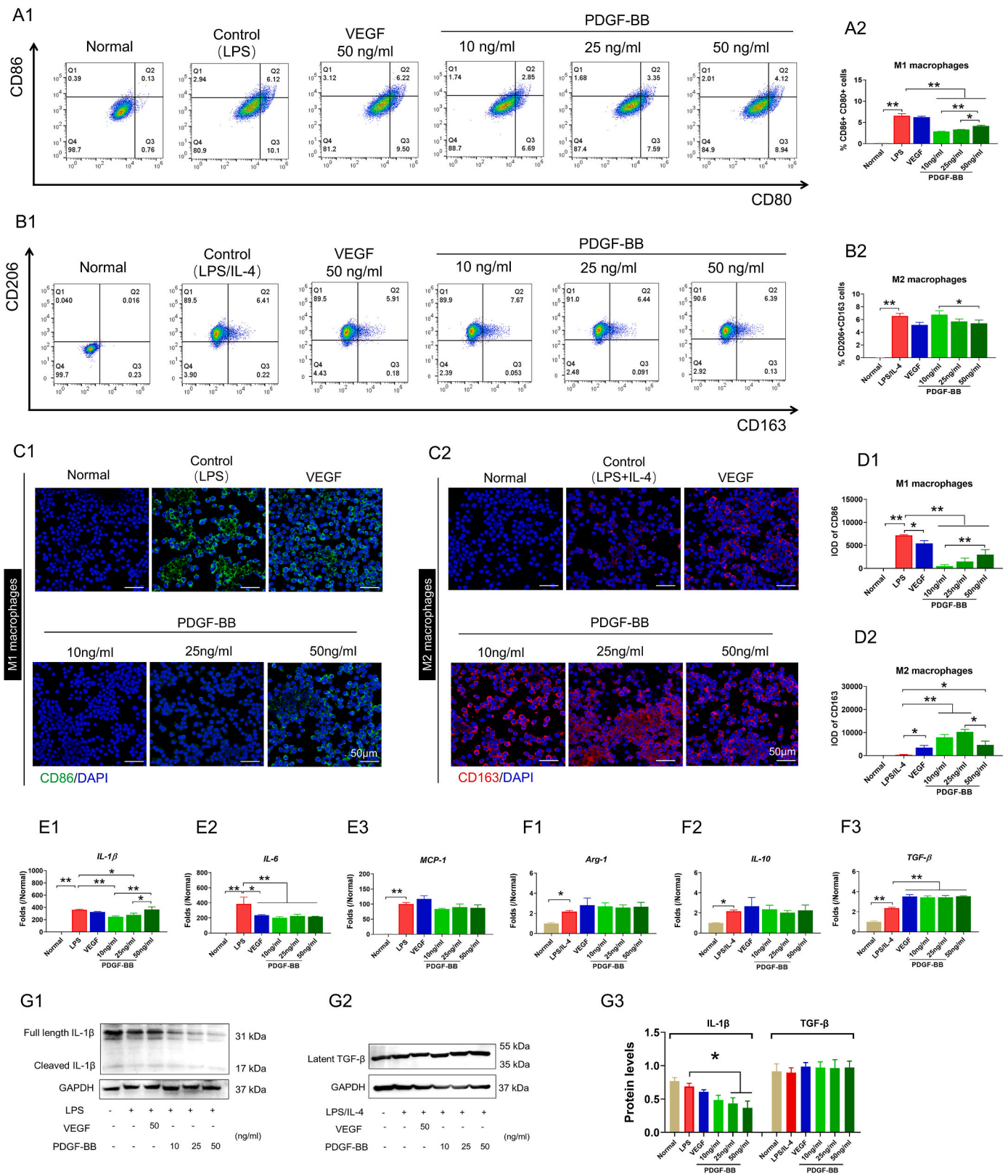

Fig. 7. PDGF-BB regulates macrophages activation. (**A1 & B1**) Measurement of the relative content of M1 (**A1**) and M2 (**B1**) subtypes of macrophages in 24 h after LPS or LPS/IL-4 stimulations and PDGF-BB treatment by flow cytometry. (**A2 & B2**) Quantification analysis data of the CD68+CD80+ cells (**A2**) and the CD163+CD206+ cells (**B2**). n=3. (**C**) RAW 264.7 cells were stimulated with LPS or LPS/IL-4 and plus PDGF-BB (10, 25 and 50 ng/ml) for 24 h, then the expressions of M1-biomarker CD86 (green, **C1**) and M2-biomarker CD163 (red, **C2**) were detected by fluorescence staining. (**D**) Quantification of the content of CD68+ cells (**D1**) and CD163+ cells (**D2**). n=3. (**E**) mRNA expression levels of *IL-1β* (**E1**), *IL-6* (**E2**) and *MCP-1* (**E3**) in RAW 264.7 cells in 12 h after LPS stimulations. n=3. (**F**) mRNA expression levels of *Arg-1* (**F1**), *IL-10* (**F2**), and *TGF-β* (**F3**) in RAW 264.7 cells in 12 h after LPS/IL-4 stimulations. n=3. (**G**) Western blot images of total IL-1*β* (**G1**), TGF-*β* (**G2**), and GAPDH in RAW 264.7 cells after LPS and/or IL-4 for 24 h, respectively. (**G3**) Quantification analysis data of the ratios of IL-1*β* and TGF-*β* which used GAPDH as a reference. n=3. The data were analyzed by the One-way ANOVA (Fisher-LSD multiple comparisons) (*$p<0.05$, **$p<0.01$).

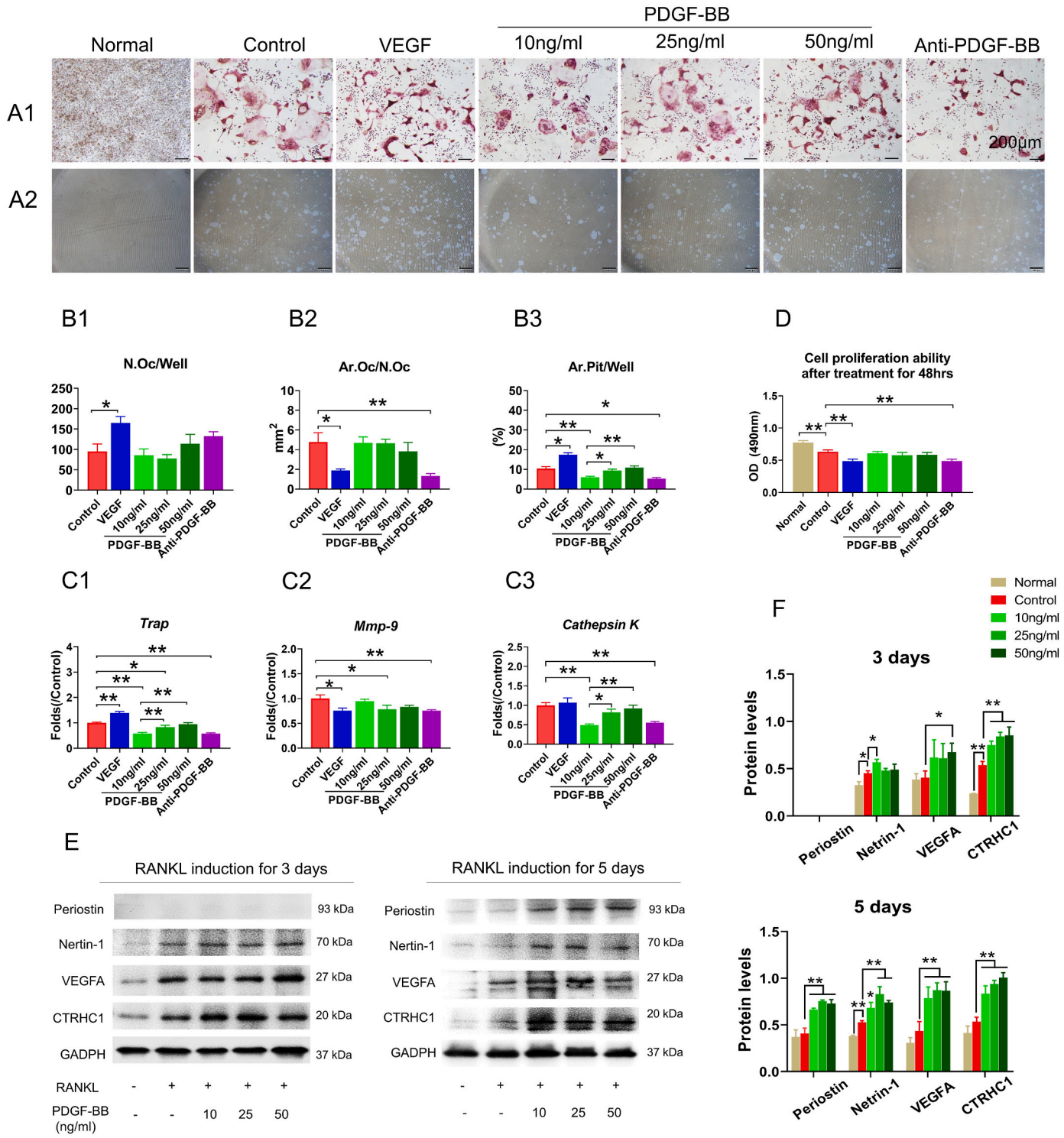

Fig. 8. PDGF-BB regulates osteoclasts formation and function, and further increases bioactivity factors expression during osteoclastogenesis process. (**A**) Representative TRAP staining images showing differentiated osteoclast morphology and number (**A1**) (bar=200 μm), and representative pit formation images showing osteoclast function on day 7 after RANKL (50 ng/ml) induction (**A2**) (bar=200 μm). (**B**) Quantitative analysis of the number of TRAP+ multinucleated cells (**B1**, N.Oc/Well), the area of TRAP+ multinucleated cells (**B2**, Ar.Oc/N.Oc), and the pit area (**B3**, Ar.Pit/Well) in each group. n=3. (**C**) mRNA expression levels of *Trap* (**C1**), *Mmp-9* (**C2**), and *Cathepsin K* (**C3**) in RAW 264.7 cells in day 7 after RANKL induction. n=4. (**D**) RAW 264.7 cells proliferation assay after RANKL induction for 2 days (48 h) by CCK-8 kit. n=8. (**E**) Western blot images of total Periostin, Netrin-1, VEGFA, CTHRC1, and GAPDH in RAW 264.7 cells after RANKL induction for 3 and 5 days, respectively. (**F**) Quantification analysis data of the ratio of Periostin, Netrin-1, VEGFA, CTHRC1 which used GAPDH as a reference. n=3. The data were analyzed by the One-way ANOVA (Fisher-LSD multiple comparisons) (*$p<0.05$, **$p<0.01$).

in ON regions [5,59]. Activated macrophages can induce the production of proinflammatory cytokines, contributing to inflammatory bone loss and impairing bone formation capacity [5]. In this study, extensive inflammatory responses were observed in the femur marrow cavity following SAON induction. While pro-inflammatory signaling is crucial for initiating the healing process and recruiting various cell types, but its timing is crucial [60]. Persistent pro-inflammatory signaling can delay or prevent healing [60]. Thus, a dynamic shift from pro-inflammatory to anti-inflammatory signaling is essential for bone regeneration, involving the phenotypic transition between M1-type and M2-type macrophages [59]. In fact, over 70 % PDGF-BB is secreted by macrophage lineage TRAP + cells in the bone tissue [61]. PDGF-BB has been reported to inhibit immune cell activation and cytokines production *in vivo* and *in vitro* [62]. Herein, our findings revealed that the application of PDGF-BB modulates the transition between M1-type and M2-type macrophages and reduces the level of the inflammatory factor IL-1β in an inflammatory environment, suggesting PDGF-BB may have a potential to promote the shift from inflammatory phase to bone remodeling phase.

Although PDGF-BB shown an excellent effect on promoting angiogenesis and osteogenesis *in vivo* [63], its direct effect on bone formation remains controversial [14]. Some evidence suggests that PDGF-BB promotes the proliferation and collagen production of osteoprogenitor cells or osteoblasts but dose not enhance osteoblastic differentiation and mineralization [64,65]. Bone healing is a highly coordinated process and orchestrated by various cells [66]. PDGF-BB serves as a chemoattractant and mitogen for endothelial cells (ECs) and MSCs, orchestrating cellular components for bone healing [67]. Our previous study found PDGF-BB increased MSCs proliferation at the expense of differentiation, and it also failed to enhance the tube formation of ECs directly *in vitro* [21]. Notably, the interaction between MSCs and ECs further regulates vascular homeostasis [68]. We also found that PDGF-BB preserved the osteogenic potential of MSCs by activating PDGFR/Akt/GSK3β/CERE signaling in the presence of GC [21], and another study proved that PDGF-BB stabilized the newly formed vascular tubes by recruiting MSCs during the bone healing cascade via PDGFR/Src/Akt signaling in the inflammatory microenvironment [67]. PDGF-BB has been reported to activate sequential bone healing and remodeling phases, starting from inflammation [63]. With regard to the macrophage lineage TRAP + cell has been showed to participate in removing necrotic bone tissue and sequentially secreting bioactive factors to couple new bone formation [69]. The communication mechanism of bone remodeling by which bone formation follows bone resorption, is known as coupling, with osteoclast-secreted coupling factors playing a crucial role [36]. Therefore, we further analyzed the expression levels about nerve and vessel regeneration associated factors Nertin-1 and VEGF-A [37], bone matrix degradation and TGF-β release associated factor CTHRC1 [38], and periosteal osteogenic associated factor Periostin [17], during the differentiation and mature processes of macrophage lineage TRAP + cells. It has been reported PDGF-BB can drive chemotaxis of osteoclast precursor cells and modulate osteoclast function by enhancing the phosphorylation of STAT3, Akt, and ERK1/2 through PDGF/PDGFR signaling pathway [70]. Our data demonstrated that PDGF-BB application upregulated Netrin-1, VEGF-A, CTHRC1 and Periostin expressions during osteoclasts differentiation and maturation processes. Interestingly, we found that a low dose of PDGF-BB (10 ng/ml) slowed the osteoclast differentiation process, yet a high dose PDGF-BB (50 ng/ml) did not enhance osteoclastic bone resorption. These findings suggest the PDGF-BB-treated TRAP + cells may prioritize providing a secondary source of growth factors rather than directly promoting bone resorption, thereby enhancing the coupling mechanism of osteoclast function with revascularization, nerve regeneration and osteogenesis.

Traditional administration of growth factors is limited by their short half-life and potential side effects [71]. PDGF-BB has a very short half-life of 2 min, which means that controlled and more sustained delivery could be required to ensure its efficient activity [72]. However, increasing evidence suggests that PDGF-BB orchestrates osteogenesis *in vivo* in a temporal manner [73], and continuous PDGF-BB stimulation may inhibit BMP-2-induced osteoblastic differentiation and mineralization [74]. In one study, continuous VEGF administration over 14 days using an osmotic micropump for treating traumatic-osteonecrosis of femoral head (induced by cryosurgical) did not yield superior outcomes compared to a single-dose injection [75]. This suggests that a high single initial dose of growth factor may be more effective for the bone healing, particularly in the initial stage of bone healing, to reconstruct a favorable osteogenic microenvironment. In this study, initial PDGF-BB application restored the osteogenic microenvironment by regulating the communications between macrophages and other bone repair cells, referring modulating M1-type and M2-type macrophages transitions, and subsequently stimulating TRAP + cells to provide a secondary source of bioactive factors for continued bone remodeling. Furthermore, the results indicated that PDGF-BB treatment at 2 μg/dose was superior to 1 μg/dose in improving cortical bone remodeling capacity, effectively restoring the balance between bone formation and resorption in the SAON-affected femur shaft. However, this study does not conclusively prove this mechanism *in vivo*, warranting further evaluation of the inflammation response and bone healing cascade following PDGF-BB application in future studies, particularly in an animal model of atypical femoral fracture (AFF) under SAON conditions.

5. Conclusion

SAON progression leads to diaphyseal cortical bone deterioration, while PDGF-BB application could restore the osteogenic microenvironment and drive cortical bone remodeling under SAON progression. These findings position PDGF-BB as a potential candidate to attenuate SAON progression. Local delivery of PDGF-BB during surgical interventions for SONFH may enhance cortical bone repair and mechanical stability, offering a clinically viable strategy to improve long-term outcomes.

Author contributions

Conception and design of study: Huijuan Cao, Xinluan Wang, Ling Qin; Acquisition of data: Huijuan Cao, Keda Shi, Jing Long, Yanzhi Liu, Cuishan Huang, Xiangbo Meng, Jie Hao, Lingli Li, Yiqing Zhao, Tianluo Ye; Analysis and/or interpretation of data: Huijuan Cao, Keda Shi, Lingli Li, Jie Hao, Yiqing Zhao; Drafting the manuscript: Huijuan Cao, Xinluan Wang; Revising the manuscript critically for important intellectual content: Xinluan Wang; Yuxiao Lai, Ling Qin; Approval of the version of the manuscript to be published (the names of all authors must be listed): Huijuan Cao, Keda Shi, Jing Long, Yanzhi Liu, Xiangbo Meng, Cuishan Huang, Jie Hao, Lingli Li, Yiqing Zhao, Tianluo Ye, Yuxiao Lai, Ling Qin, Xinluan Wang.

Data availability statement

The data that support the findings of this study are available from the corresponding author upon reasonable request.

Declaration of competing interest

The authors declare no conflict of interests.

Acknowledgments

This work was supported by National Key R&D Program of China (2023YFC2509900), National Natural Science Foundation of China (U22A20371), and Science, Technology and Innovation Commission of Shenzhen (JCYJ20210324102006017).

Appendix A. Supplementary data

Supplementary data to this article can be found online at https://doi.org/10.1016/j.jot.2025.03.010.

References

[1] Chaudhuri D, Nei AM, Rochwerg B, Balk RA, Asehnoune K, Cadena R, et al. Focused update: Guidelines on use of corticosteroids in sepsis, acute respiratory distress syndrome, and community-acquired pneumonia. Crit Care Med 2024;52(5):e219–33.
[2] Hua C, Buttgereit F, Combe B. Glucocorticoids in rheumatoid arthritis: current status and future studies. RMD Open 2020;6(1):e000536.
[3] Mont MA, Pivec R, Banerjee S, Issa K, Elmallah RK, Jones LC. High-dose corticosteroid use and risk of hip osteonecrosis: meta-analysis and systematic literature review. J Arthroplast 2015;30(9):1506–1512.e1505.
[4] Kaneko K, Chen H, Kaufman M, Sverdlov I, Stein EM, Park-Min KH. Glucocorticoid-induced osteonecrosis in systemic lupus erythematosus patients. Clin Transl Med 2021;11(10):e526.
[5] Goodman SB, Maruyama M. Inflammation, bone healing and osteonecrosis: from bedside to bench. J Inflamm Res 2020;13:913–23.
[6] Dhanasekararaja P, Soundarrajan D, Kumar KS, Pushpa BT, Rajkumar N, Rajasekaran S. Aggressive presentation and rapid progression of osteonecrosis of the femoral head after COVID-19. Indian J Orthop 2022;56(7):1259–67.
[7] Hua KC, Yang XG, Feng JT, Wang F, Yang L, Zhang H, et al. The efficacy and safety of core decompression for the treatment of femoral head necrosis: a systematic review and meta-analysis. J Orthop Surg Res 2019;14(1):306.
[8] Waewsawangwong W, Ruchiwit P, Huddleston JI, Goodman SB. Hip arthroplasty for treatment of advanced osteonecrosis: comprehensive review of implant options, outcomes and complications. Orthop Res Rev 2016;8:13–29.
[9] Nishino T, Hyodo K, Matsumoto Y, Yanagisawa Y, Yamazaki M. Bisphosphonate-related atypical femoral fractures in patients with autoimmune disease treated with glucocorticoids: surgical results for 20 limbs. J Clin Med 2024;13(4):1027.
[10] Rahman WA, Garbuz DS, Masri BA. Total hip arthroplasty in steroid-induced osteonecrosis: early functional and radiological outcomes. Can J Surg 2013;56(1):41–6.
[11] Salman LA, Hantouly AT, Khatkar H, Al-Ani A, Abudalou A, Al-Juboori M, et al. The outcomes of total hip replacement in osteonecrosis versus osteoarthritis: a systematic review and meta-analysis. Int Orthop 2023;47(12):3043–52.
[12] Calder JD, Pearse MF, Revell PA. The extent of osteocyte death in the proximal femur of patients with osteonecrosis of the femoral head. The Journal of bone and joint surgery British 2001;83(3):419–22.
[13] Gillman CE, Jayasuriya AC. FDA-approved bone grafts and bone graft substitute devices in bone regeneration. Mater Sci Eng C 2021;130:112466.
[14] Graham S, Leonidou A, Lester M, Heliotis M, Mantalaris A, Tsiridis E. Investigating the role of PDGF as a potential drug therapy in bone formation and fracture healing. Expet Opin Invest Drugs 2009;18(11):1633–54.
[15] Martinez CE, Smith PC, Palma Alvarado VA. The influence of platelet-derived products on angiogenesis and tissue repair: a concise update. Front Physiol 2015;6:290.
[16] Sivaraj KK, Jeong HW, Dharmalingam B, Zeuschner D, Adams S, Potente M, et al. Regional specialization and fate specification of bone stromal cells in skeletal development. Cell Rep 2021;36(2):109352.
[17] Gao B, Deng R, Chai Y, Chen H, Hu B, Wang X, et al. Macrophage-lineage TRAP+ cells recruit periosteum-derived cells for periosteal osteogenesis and regeneration. J Clin Investig 2019;129(6):2578–94.
[18] Peng Y, Lv S, Li Y, Zhu J, Chen S, Zhen G, et al. Glucocorticoids disrupt skeletal angiogenesis through transrepression of NF-kappaB-Mediated preosteoclast Pdgfb transcription in young mice. J Bone Miner Res 2020;35(6):1188–202.
[19] Jia Y, Zhang Y, Li S, Li R, Li W, Li T, et al. Identification and assessment of novel dynamic biomarkers for monitoring non-traumatic osteonecrosis of the femoral head staging. Clin Transl Med 2023;13(6):e1295.
[20] Zhang G, Sheng H, He YX, Xie XH, Wang YX, Lee KM, et al. Continuous occurrence of both insufficient neovascularization and elevated vascular permeability in rabbit proximal femur during inadequate repair of steroid-associated osteonecrotic lesions. Arthritis Rheum 2009;60(10):2966–77.
[21] Cao H, Shi K, Long J, Liu Y, Li L, Ye T, et al. PDGF-BB prevents destructive repair and promotes reparative osteogenesis of steroid-associated osteonecrosis of the femoral head in rabbits. Bone 2022;167:116645.
[22] Li Y, Chen SK, Li L, Qin L, Wang XL, Lai YX. Bone defect animal models for testing efficacy of bone substitute biomaterials. J Orthop Translat 2015;3(3):95–104.
[23] Permuy M, Lopez-Pena M, Munoz F, Gonzalez-Cantalapiedra A. Rabbit as model for osteoporosis research. J Bone Miner Metabol 2019;37(4):573–83.
[24] Blanc-Sylvestre N, Bouchard P, Chaussain C, Bardet C. Pre-clinical models in implant dentistry: past, present, future. Biomedicines 2021;9(11).
[25] Long J, Yao Z, Zhang W, Liu B, Chen K, Li L, et al. Regulation of osteoimmune microenvironment and osteogenesis by 3D-printed PLAG/black phosphorus scaffolds for bone regeneration. Adv Sci 2023;10(28):e2302539.
[26] Zhou H, Wang DA, Baldini L, Ennis E, Jain R, Carie A, et al. Structure-activity studies on a library of potent calix[4]arene-based PDGF antagonists that inhibit PDGF-stimulated PDGFR tyrosine phosphorylation. Org Biomol Chem 2006;4(12):2376–86.
[27] Tsugeno H, Goto B, Fujita T, Okamoto M, Mifune T, Mitsunobu F, et al. Oral glucocorticoid-induced fall in cortical bone volume and density in postmenopausal asthmatic patients. Osteoporos Int 2001;12(4):266–70.
[28] Li L, Yi X, Huang C, Shi K, Wang J, Zeng Q, et al. Qu Feng Zhi Tong capsule increases mechanical properties of cortical bone in ovariectomised rats. J Orthop Transl 2020;25:115–24.
[29] Varga Z, Flammer AJ, Steiger P, Haberecker M, Andermatt R, Zinkernagel AS, et al. Endothelial cell infection and endotheliitis in COVID-19. Lancet 2020;395(10234):1417–8.
[30] Zheng GS, Qiu X, Wang BJ, Zhao DW. Relationship between blood flow and collapse of nontraumatic osteonecrosis of the femoral head. J Bone Joint Surg Am 2022;104(Suppl 2):13–8.
[31] Wang A, Ren M, Wang J. The pathogenesis of steroid-induced osteonecrosis of the femoral head: a systematic review of the literature. Gene 2018;671:103–9.
[32] Zhou BO, Yue R, Murphy MM, Peyer JG, Morrison SJ. Leptin-receptor-expressing mesenchymal stromal cells represent the main source of bone formed by adult bone marrow. Cell Stem Cell 2014;15(2):154–68.
[33] Torres HM, Arnold KM, Oviedo M, Westendorf JJ, Weaver SR. Inflammatory processes affecting bone health and repair. Curr Osteoporos Rep 2023;21(6):842–53.
[34] Zhang Q, Sun W, Li T, Liu F. Polarization behavior of bone macrophage as well as associated osteoimmunity in glucocorticoid-induced osteonecrosis of the femoral head. J Inflamm Res 2023;16:879–94.
[35] Ishida K, Nagatake T, Saika A, Kawai S, Node E, Hosomi K, et al. Induction of unique macrophage subset by simultaneous stimulation with LPS and IL-4. Front Immunol 2023;14:1111729.
[36] Sims NA, Martin TJ. Osteoclasts provide coupling signals to osteoblast lineage cells through multiple mechanisms. Annu Rev Physiol 2020;82:507–29.
[37] Zhu S, Zhu J, Zhen G, Hu Y, An S, Li Y, et al. Subchondral bone osteoclasts induce sensory innervation and osteoarthritis pain. J Clin Investig 2019;129(3):1076–93.
[38] Takeshita S, Fumoto T, Matsuoka K, Park KA, Aburatani H, Kato S, et al. Osteoclast-secreted CTHRC1 in the coupling of bone resorption to formation. J Clin Investig 2013;123(9):3914–24.
[39] Fu W, Liu B, Wang B, Zhao D. Early diagnosis and treatment of steroid-induced osteonecrosis of the femoral head. Int Orthop 2019;43(5):1083–7.
[40] Qin L, Zhang G, Sheng H, Yeung KW, Yeung HY, Chan CW, et al. Multiple bioimaging modalities in evaluation of an experimental osteonecrosis induced by a combination of lipopolysaccharide and methylprednisolone. Bone 2006;39(4):863–71.
[41] Zheng LZ, Cao HJ, Chen SH, Tang T, Fu WM, Huang L, et al. Blockage of Src by specific siRNA as a novel therapeutic strategy to prevent destructive repair in steroid-associated osteonecrosis in rabbits. J Bone Miner Res 2015;30(11):2044–57.
[42] Huang C, Wen Z, Niu J, Lin S, Wang W. Steroid-induced osteonecrosis of the femoral head: novel insight into the roles of bone endothelial cells in pathogenesis and treatment. Front Cell Dev Biol 2021;9:777697.
[43] Saita Y, Ishijima M, Kaneko K. Atypical femoral fractures and bisphosphonate use: current evidence and clinical implications. Ther Adv Chronic Dis 2015;6(4):185–93.
[44] Schilcher J, Sandberg O, Isaksson H, Aspenberg P. Histology of 8 atypical femoral fractures: remodeling but no healing. Acta Orthop 2014;85(3):280–6.
[45] Aeberli D, Schett G. Cortical remodeling during menopause, rheumatoid arthritis, glucocorticoid and bisphosphonate therapy. Arthritis Res Ther 2013;15(2).
[46] Szulc P, Seeman E, Duboeuf F, Sornay-Rendu E, Delmas PD. Bone fragility: failure of periosteal apposition to compensate for increased endocortical resorption in postmenopausal women. J Bone Miner Res 2006;21(12):1856–63.
[47] Li X, Liang T, Dai B, Chang L, Zhang Y, Hu S, et al. Excess glucocorticoids inhibit murine bone turnover via modulating the immunometabolism of the skeletal microenvironment. J Clin Investig 2024;134(10).
[48] Ding M, Cheng L, Bollen P, Schwarz P, Overgaard S. Glucocorticoid induced osteopenia in cancellous bone of sheep: validation of large animal model for spine fusion and biomaterial research. Spine 2010;35(4):363–70.
[49] Ding M, Danielsen CC, Overgaard S. The effects of glucocorticoid on microarchitecture, collagen, mineral and mechanical properties of sheep femur cortical bone. J Tissue Eng Regen Med 2012;6(6):443–50.
[50] Harrison KD, Hiebert BD, Panahifar A, Andronowski JM, Ashique AM, King GA, et al. Cortical bone porosity in rabbit models of osteoporosis. J Bone Miner Res 2020;35(11):2211–28.
[51] Zheng LZ, Wang XL, Cao HJ, Chen SH, Huang L, Qin L. Src siRNA prevents corticosteroid-associated osteoporosis in a rabbit model. Bone 2016;83:190–6.
[52] Gangji V, Soyfoo MS, Heuschling A, Afzali V, Moreno-Reyes R, Rasschaert J, et al. Non traumatic osteonecrosis of the femoral head is associated with low bone mass. Bone 2018;107:88–92.
[53] Bauer DC, Black DM, Dell R, Fan B, Smith CD, Ernst MT, et al. Bisphosphonate use and risk of atypical femoral fractures: a Danish case cohort study with blinded radiographic review. J Clin Endocrinol Metab 2024.
[54] Nishino T, Hyodo K, Matsumoto Y, Yanagisawa Y, Yoshizawa T, Yamazaki M. Surgical results of atypical femoral fractures in long-term bisphosphonate and glucocorticoid users - relationship between fracture reduction and bone union. J Orthop 2020;19:143–9.
[55] Egol KA, Park JH, Rosenberg ZS, Peck V, Tejwani NC. Healing delayed but generally reliable after bisphosphonate-associated complete femur fractures treated with IM nails. Clin Orthop Relat Res 2014;472(9):2728–34.
[56] Daniels TR, Anderson J, Swords MP, Maislin G, Donahue R, Pinsker E, et al. Recombinant human platelet-derived growth factor BB in combination with a beta-

tricalcium phosphate (rhPDGF-BB/beta-TCP)-Collagen matrix as an alternative to autograft. Foot Ankle Int 2019;40(9):1068–78.
[57] Hollinger JO, Onikepe AO, MacKrell J, Einhorn T, Bradica G, Lynch S, et al. Accelerated fracture healing in the geriatric, osteoporotic rat with recombinant human platelet-derived growth factor-BB and an injectable beta-tricalcium phosphate/collagen matrix. J Orthop Res 2008;26(1):83–90.
[58] Al-Zube L, Breitbart EA, O'Connor JP, Parsons JR, Bradica G, Hart CE, et al. Recombinant human platelet-derived growth factor BB (rhPDGF-BB) and beta-tricalcium phosphate/collagen matrix enhance fracture healing in a diabetic rat model. J Orthop Res 2009;27(8):1074–81.
[59] Zheng J, Yao Z, Xue L, Wang D, Tan Z. The role of immune cells in modulating chronic inflammation and osteonecrosis. Front Immunol 2022;13:1064245.
[60] Duda GN, Geissler S, Checa S, Tsitsilonis S, Petersen A, Schmidt-Bleek K. The decisive early phase of bone regeneration. Nat Rev Rheumatol 2023;19(2):78–95.
[61] Xie H, Cui Z, Wang L, Xia Z, Hu Y, Xian L, et al. PDGF-BB secreted by preosteoclasts induces angiogenesis during coupling with osteogenesis. Nat Med 2014;20(11):1270–8.
[62] Wang M, Wei J, Shang F, Zang K, Ji T. Platelet-derived growth factor B attenuates lethal sepsis through inhibition of inflammatory responses. Int Immunopharmacol 2019;75:105792.
[63] DiGiovanni CW, Glazebrook M, Snel LB, Beasley B, Lynch SE, Friedlaender GE. A review of the clinical experience with recombinant human platelet-derived growth factor-BB (rhPDGF-BB) in orthopaedic bone repair and regeneration. Curr Orthop Pract 2013;24(5):476–81.
[64] Qu B, Xia X, Wu HH, Tu CQ, Pan XM. PDGF-regulated miRNA-138 inhibits the osteogenic differentiation of mesenchymal stem cells. Biochem Biophys Res Commun 2014;448(3):241–7.
[65] Park SY, Kim KH, Shin SY, Koo KT, Lee YM, Seol YJ. Dual delivery of rhPDGF-BB and bone marrow mesenchymal stromal cells expressing the BMP2 gene enhance bone formation in a critical-sized defect model. Tissue Eng Part A 2013;19(21–22):2495–505.
[66] ElHawary H, Baradaran A, Abi-Rafeh J, Vorstenbosch J, Xu L, Efanov JI. Bone healing and inflammation: principles of fracture and repair. Semin Plast Surg 2021;35(3):198–203.
[67] He S, Hou T, Zhou J, Ai Q, Dou C, Luo F, et al. Endothelial cells promote migration of mesenchymal stem cells via PDGF-BB/PDGFRβ-Src-Akt in the context of inflammatory microenvironment upon bone defect. Stem Cell Int 2022;2022:2401693.
[68] Bronckaers A, Hilkens P, Martens W, Gervois P, Ratajczak J, Struys T, et al. Mesenchymal stem/stromal cells as a pharmacological and therapeutic approach to accelerate angiogenesis. Pharmacol Ther 2014;143(2):181–96.
[69] Chen K, Jiao Y, Liu L, Huang M, He C, He W, et al. Communications between bone marrow macrophages and bone cells in bone remodeling. Front Cell Dev Biol 2020;8:598263.
[70] Li DQ, Wan QL, Pathak JL, Li ZB. Platelet-derived growth factor BB enhances osteoclast formation and osteoclast precursor cell chemotaxis. J Bone Miner Metabol 2017;35(4):355–65.
[71] Kuroda Y, Kawai T, Goto K, Matsuda S. Clinical application of injectable growth factor for bone regeneration: a systematic review. Inflamm Regen 2019;39:20.
[72] Bowen-Pope DF, Raines EW. History of discovery: platelet-derived growth factor. Arterioscler Thromb Vasc Biol 2011;31(11):2397–401.
[73] Wang F, Ye Y, Zhang Z, Teng W, Sun H, Chai X, et al. PDGFR in PDGF-BB/PDGFR signaling pathway does orchestrates osteogenesis in a temporal manner, vol. 6. Research (Wash D C); 2023. p. 86.
[74] Novak S, Madunic J, Shum L, Vucetic M, Wang X, Tanigawa H, et al. PDGF inhibits BMP2-induced bone healing. NPJ Regen Med 2023;8(1):3.
[75] Zoe Dailiana, Nikolaos Stefanou, Lubna Khaldi, et al. Vascular endothelial growth factor for the treatment of femoral head osteonecrosis: an experimental study in canines. World J Orthoped 2018.